

Non-Fermi Liquid and Fermi Liquid in Two-Channel Anderson Lattice Model: Theory for $\text{Pr}A_2\text{Al}_{20}$ ($A=\text{V, Ti}$) and $\text{PrIr}_2\text{Zn}_{20}$

Atsushi Tsuruta¹ and Kazumasa Miyake^{1,2}

¹*Division of Materials Physics, Department of Materials Engineering Science, Graduate School of Engineering Science, Osaka University, Toyonaka, Osaka 560-8531, Japan*

²*Toyota Physical and Chemical Research Institute, Nagakute, Aichi 480-1192, Japan*

(Received December 7, 2024)

We theoretically investigate electronic states and physical properties in a two-channel Anderson lattice model to understand the non-Fermi liquid behaviors observed in $\text{PrV}_2\text{Al}_{20}$ and $\text{PrIr}_2\text{Zn}_{20}$ whose ground state of the crystalline electric field for local f -electron is the Γ_3 non-Kramers doublet of f^2 -configuration and excited state is the Γ_7 Kramers doublet of f^1 -configuration. We use the expansion from the limit of large degeneracy N of the ground state ($1/N$ -expansion), with N being the spin-orbital degeneracy. Inclusion of the self-energy of the conduction electrons up to the order of $O(1/N)$ leads to heavy electron with channel and spin-orbit degeneracies. We find that the electrical resistivity is proportional to temperature T in the limit of $T \rightarrow 0$ and follows \sqrt{T} -law in the wide region of temperature, i.e., $T_x < T < T_0$, where typical values of T_x and T_0 are $T_x \sim 10^{-3}T_K$ and $T_0 \sim 10^{-2}T_K$, respectively, T_K being the Kondo temperature of the model. We also find non-Fermi liquid behaviors at $T \ll T_K$ in a series of physical quantities; the chemical potential, the specific heat, and the magnetic susceptibility, explaining the non-Fermi liquid behaviors observed in $\text{PrV}_2\text{Al}_{20}$ and $\text{PrIr}_2\text{Zn}_{20}$. At the same time, we find that the Fermi liquid behavior becomes prominent for the system with smaller hybridization between f - and conduction electrons, explaining the Fermi liquid behaviors observed in $\text{PrTi}_2\text{Al}_{20}$.

1. Introduction

Recently, non-Fermi liquid behaviors in the resistivity $\rho(T)$ have been reported in $\text{PrV}_2\text{Al}_{20}$ ¹⁾ and $\text{PrIr}_2\text{Zn}_{20}$.²⁾ Namely, the electrical resistivity is proportional to \sqrt{T} in rather wide temperature region. The specific heat $C(T)$ and the magnetic susceptibility $\chi_m(T)$ increase like (const. $- \sqrt{T}$) toward T_Q , the transition temperature of quadrupolar

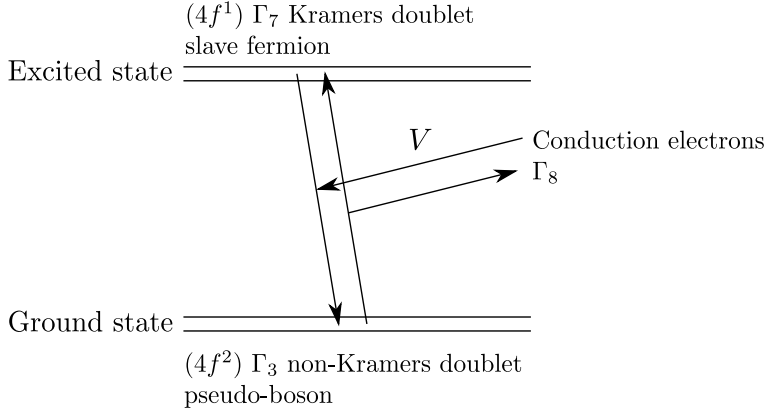


Fig. 1. Levels scheme of f -electrons and hybridization path with conduction electrons of model Hamiltonian, Eqs. (2)-(5).

ordering, as T decreases below Kondo temperature, T_K , which is a fundamental energy scale characterizing the physics. The anomaly in the specific heat and the cusp in the magnetic susceptibility are also observed in PrPb_3 .³⁾ From analyses of the specific heat, magnetic moment, and inelastic neutron scattering experiment, the ground state of the crystalline-electrical field (CEF) of the local f -electron is considered to be the Γ_3 non-Kramers doublet in $4f^2$ -configuration,²⁾ as shown in Fig. 1.

Such a system with the Γ_3 CEF ground state in f^2 -configuration is expected to exhibit an anomalous behaviors associated with the two-channel Kondo effect. Indeed, the two-channel Kondo model (proposed by Nozières and Blandin⁴⁾) revived a quarter century ago when Cox proposed it as a realistic model for explaining anomalous non-Fermi liquid properties of cubic heavy fermion metal UBe_{13} on the basis of the quadrupolar Kondo effect.⁵⁾ Since then, the two-channel Kondo problem has been attracting much attention.⁶⁾

On the other hand, strong electronic correlation has been widely believed to play a crucial role in the generation of the heavy electrons observed in rare-earth and actinide based metals as well as the various anomalous phenomena observed in high- T_c cuprate superconductors. For simulation of such systems with strong electronic correlation, various types of Anderson models have been used. One of the powerful methods to properly treat these models is that based on the expansion from the limit of the large spin-orbital degeneracy N (1/ N -expansion method).

Ōno *et al.*⁷⁾ have treated the conventional (single-channel) Anderson lattice model by the 1/ N -expansion method in the leading order of 1/ N , and have succeeded in

describing the heavy Fermi liquid state in which the Luttinger sum rule holds. Various Fermi liquid properties of the lattice model have been discussed along this formulation by taking into account higher-order terms in $1/N$.^{8,9)} Tsuruta *et al.*^{10,11)} have also confirmed, in the single-channel Anderson lattice model, that the imaginary part of the self-energy of conduction electrons is given by the form $\text{Im}\Sigma(\epsilon + i0_+) = -\alpha[\epsilon^2 + (\pi T)^2]$, α being a constant proportional to T_K^{-2} , up to $O(N^{-2})$ in the regions of frequency $|\epsilon| \ll T_K$ and of temperature $T \ll T_K$, and that the Luttinger sum rule holds up to $O(N^{-1})$. Furthermore, it has been confirmed that $\text{Im}\Sigma(\epsilon + i0_+) \propto -\ln[\max(|\epsilon|, T)]$ at $\max(|\epsilon|, T) > T_K$, implying that the Kondo effect at $T > T_K$ is reproduced.^{10,11)} Namely, this version of $1/N$ -expansion method is a powerful method for investigating essential properties of the Anderson lattice model.

On this formalism, Nishida *et al.*¹²⁾ have investigated effects of the CEF level splitting on the resistivity of Ce-based compound taking account of the self-energy up to $O(1/N)$, and have explained the T dependence of the resistivity in $\text{CeCu}_2(\text{Si,Ge})_2$ which exhibit the double peak structure in its T dependence at ambient pressure. They have also shown that the double peaks merge into a single peak as the c - f hybridization increases, explaining such a mergence under pressure observed in $\text{CeCu}_2(\text{Si,Ge})_2$ ^{13,14)} and some other heavy fermion systems, such as CeAl_2 .¹⁵⁾

Properties of the two-channel Kondo lattice model in infinite dimensions have been studied by Jarrell *et al.*¹⁶⁾ with the use of a quantum Monte Carlo simulation. It has been found that the resistivity $\rho(T)$ is finite even at $T = 0$, which is apparently unphysical. This unphysical result have occurred since the translational symmetry was not properly taken in account in their study which relies on a property of infinite dimensions. In infinite dimensions, the inter-site correlation effects on the self-energy of the conduction electrons are inevitably neglected.

On the basis of the $1/N$ -expansion formalism, Tsuruta *et al.*¹⁰⁾ have shown, in the two-channel Anderson model shown in Fig. 1, that the imaginary part of the self-energy of conduction electrons, is proportional to T in the limit of $T \rightarrow 0$ up to $O(1/N)$, if the inter-site effects on the self-energy are properly taken into account. Indeed, the imaginary part of the self-energy of conduction electrons, at $|\epsilon| \ll T_K$ and $T \ll T_K$, is given in the form

$$\text{Im}\Sigma_{\mathbf{k}}(\epsilon + i0_+) = -\pi\alpha_{\mathbf{k}}^{(1)}[\epsilon^2 + (\pi T)^2] - \pi\frac{\beta_{\mathbf{k}}^{(1)}}{1 + T_{\mathbf{k}}^*/T}(1 - M^{-2}), \quad (1)$$

where $T_{\mathbf{k}}^*$ is the temperature characterizing the non-Fermi liquid state, and $\alpha_{\mathbf{k}}^{(1)}$ and $\beta_{\mathbf{k}}^{(1)}$ are constants proportional to $N_F V^2 T_K^{-2}$ and N_F^{-1} , respectively, where V and N_F are c - f hybridization and the density of states of conduction electrons at the Fermi level. The imaginary part with $\epsilon = 0$ is proportional to T in the limit $T \rightarrow 0$ in the leading order of T , i.e., it exhibits the non-Fermi-liquid-type behavior, and furthermore, in rather wide temperature region of $T < T_K$, it behaves as $\text{Im}\Sigma_{\mathbf{k}}(i0_+) \propto \sqrt{TT_K}$. Thus, the T - and ϵ -dependence of $\text{Im}\Sigma_{\mathbf{k}}(\epsilon + i0_+)$ given by Eq. (1) seem to have a potential for explaining anomalous properties observed in $\text{PrV}_2\text{Al}_{20}$ ¹⁾ and $\text{PrIr}_2\text{Zn}_{20}$.²⁾

In the present paper, we follow the idea that these Pr-based compounds are realization of the two-channel Anderson lattice model, and investigate the non-Fermi liquid behavior of the two-channel Anderson lattice model by calculating the T dependence of the electrical resistivity, the chemical potential, the specific heat, and the magnetic susceptibility in the low temperature region $T < T_K$. In Sect. 2, we briefly review discussions of Ref. 11; i.e., we show the model and the formulation, and explicitly calculate the vertices and the self-energy for conduction electrons. In Sects. 3, 4, 6, and 7, we calculate T dependence of the chemical potential $\mu(T)$, the electrical resistivity $\rho(T)$, the specific heat $C(T)$, and the magnetic susceptibility $\chi_m(T)$, respectively. In Sect. 5, we analyze the origin of the difficulty of the dynamical mean field theory (DMFT) when applied to the multichannel Anderson lattice model. In Appendix A, we show the formalism for calculating the specific heat in terms of the renormalized Green function of conduction electrons, pseudo bosons, and slave fermions. A recipe for numerical calculations is given in Appendix B.

2. Review of the Previous Investigation for the Two-channel Anderson Lattice Model

2.1 Model and Formal Preliminaries

As shown in Fig. 1, we introduce an Anderson lattice model for Pr1-2-20 compounds, whose CEF ground state of f-electrons is the Γ_3 non-Kramers doublet in f^2 -configuration, as follows:

$$H = H_c + H_f + H_v \quad (2)$$

$$H_c = \sum_{\sigma=1}^M \sum_{\tau_1, \tau_2=1}^N \sum_{\mathbf{k}} \varepsilon_{\mathbf{k}\tau_1\tau_2} c_{\mathbf{k}\tau_1\sigma}^+ c_{\mathbf{k}\tau_2\sigma} \quad (3)$$

$$H_f = \sum_i \sum_{\tau=1}^N \varepsilon_{\Gamma_3}^{(0)} |f^2 : i\tau\rangle \langle f^2 : i\tau| + \sum_i \sum_{\sigma=1}^M \varepsilon_{\Gamma_7}^{(0)} |f^1 : i\sigma\rangle \langle f^1 : i\sigma| \quad (4)$$

$$H_v = \frac{1}{\sqrt{N_L}} \sum_{\mathbf{k}i} \sum_{\tau\sigma} (V e^{-i\mathbf{k}\mathbf{R}_i} c_{\mathbf{k}\tau\bar{\sigma}}^+ |f^1 : i\sigma\rangle \langle f^2 : i\tau| + \text{h.c.}) , \quad (5)$$

where σ and τ denote components of the spin-orbital degeneracy $M (= 2)$ of the Γ_7 and Γ_8 CEF state in f^1 -configuration and the quadrupole moment $N (= 2)$ of the Γ_3 CEF state in f^2 -configuration, respectively; $c_{\mathbf{k}\sigma\tau}$ represents the annihilation operator of a conduction electron with wave vector \mathbf{k} , spin-orbital σ , and quadrupole moment τ ; $|f^2 : i\tau\rangle$ is f^2 state with τ at i -site, and $|f^1 : i\sigma\rangle$ is f^1 state with σ at i -site; V represents the hybridization transforming from $|f^2 : i\tau\rangle$ to $|f^1 : i\sigma\rangle \otimes c_{\mathbf{k}\bar{\sigma}\tau}$ and vice versa (see Fig. 1); and N_L is the total number of lattice sites. Hereafter, we call σ the channel degrees of freedom and τ the pseudo-spin degrees of freedom. With the use of pseudo particles we can rewrite the Hamiltonian given by Eq. (2) as

$$\begin{aligned} H = & \sum_{\sigma=1}^M \sum_{\tau_1, \tau_2=1}^N \sum_{\mathbf{k}} \varepsilon_{\mathbf{k}\tau_1\tau_2} c_{\mathbf{k}\tau_1\sigma}^+ c_{\mathbf{k}\tau_2\sigma} + \sum_i \sum_{\tau=1}^N \varepsilon_{\Gamma_3}^{(0)} b_{i\tau}^+ b_{i\tau} + \sum_i \sum_{\sigma=1}^M \varepsilon_{\Gamma_7}^{(0)} f_{i\sigma}^+ f_{i\sigma} \\ & + \frac{1}{\sqrt{N_L}} \sum_{\sigma=1}^M \sum_{\tau=1}^N \sum_{i, \mathbf{k}} (V c_{\mathbf{k}\tau\bar{\sigma}}^+ b_{i\tau} f_{i\sigma}^+ e^{-i\mathbf{k}\mathbf{R}_i} + \text{h.c.}) , \end{aligned} \quad (6)$$

where we have introduced the pseudo boson annihilation operator $b_{i\tau}$ for representing $|f^2 : i\tau\rangle$ state and the slave fermion annihilation operator $f_{i\sigma}$ for representing $|f^1 : i\sigma\rangle$ state. Although we mainly investigate the case of two channel ($M = 2$) in the present paper, the case of the single channel ($M = 1$) is also discussed for comparison. In the latter case, both the ground state of f^1 -configuration and the conduction electrons are specified by a Kramers doublet with σ and the excited state is in f^0 -configuration, in contrast to the situation of Fig. 1. While $\varepsilon_{\mathbf{k}\tau\bar{\sigma}} \neq 0$ in general, there occurs no qualitative difference from the case of $\varepsilon_{\mathbf{k}\tau\bar{\sigma}} = 0$. Thus, in the present paper we restrict our discussion to the case of $\varepsilon_{\mathbf{k}\tau\bar{\sigma}} = 0$.

For guaranteeing the equivalence between the transformed model [Eq. (6)] and the original model [Eq. (2)] the Hamiltonian [Eq. (6)] must be treated within the subspace where the local constraint,

$$\hat{Q}_i = \sum_{\tau} b_{i\tau}^+ b_{i\tau} + \sum_{\sigma} f_{i\sigma}^+ f_{i\sigma} = 1 , \quad (7)$$

is fulfilled. In order to calculate physical quantities within the subspace restricted by the

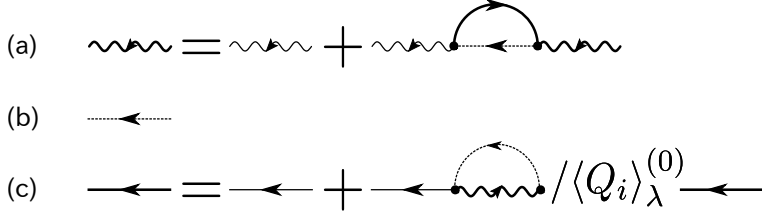


Fig. 2. Feynman diagram representation of the Dyson equations for the single-particle Green functions of the order of $O((1/N)^0)$: (a) $F_{i\sigma}^{(0)}(i\epsilon_n)$ for the slave-fermion, (b) $B_{i\tau}^{(0)}(i\nu_n)$ for the pseudo boson, and (c) $G_{k\tau\sigma}^{(0)}(i\epsilon_n)$ for the conduction electron.

local constraint [Eq. (7)], we evaluate the expectation value $\langle \hat{A} \rangle$ of a physical quantity \hat{A} such that^{18,19)}

$$\langle \hat{A} \rangle = \lim_{\{\lambda_i\} \rightarrow \infty} \left(\langle \hat{A} \Pi_i \hat{Q}_i \rangle_\lambda / \langle \Pi_i \hat{Q}_i \rangle_\lambda \right), \quad (8)$$

where

$$\langle \hat{A} \Pi_i \hat{Q}_i \rangle_\lambda \equiv \text{Tr}[e^{-\beta H_\lambda} \hat{A} \Pi_i \hat{Q}_i] / Z_\lambda, \quad (9)$$

with

$$Z_\lambda \equiv \text{Tr}[e^{-\beta H_\lambda}] \quad (10)$$

$$H_\lambda \equiv H + \sum_i \lambda_i \hat{Q}_i. \quad (11)$$

In order to calculate Eq. (8) explicitly, we employ the perturbation expansion in power of $1/N$ following the rules as

$$\frac{1}{N_L} \sum_\tau \sum_{\mathbf{k}} 1 = O((1/N)^0), \quad (12)$$

and

$$\frac{1}{N_L} \sum_{\mathbf{k}} 1 = O(1/N). \quad (13)$$

In Refs. 7 and 12 one can see the validity of this rule of power counting in $1/N$ and its physical meaning behind it. For explicit calculation in the present paper, we set $N = 2$, which may not lose the generality because we do not use the condition $1/N \ll 1$ explicitly.

2.2 Self-energy of $O((1/N)^0)$

By including terms of the order of $(1/N)^0$, the Green functions for the slave fermion $F_{i\sigma}^0(i\epsilon_n) = (i\epsilon_n - \lambda_i - \varepsilon_{\Gamma_7})^{-1}$, where $\varepsilon_{\Gamma_7} = \varepsilon_{\Gamma_7}^{(0)} - \mu$, with μ being the chemical potential,

and conduction electrons $G_{\mathbf{k}\tau\sigma}^0(i\epsilon_n) = (i\epsilon_n - \xi_{\mathbf{k}})^{-1}$, where $\xi \equiv \varepsilon_{\mathbf{k}} - \mu$, are renormalized by the effect of self-energies as illustrated in Fig. 2, while the Green function for the pseudo boson $B_{i\tau}^0(i\nu_n) = (i\nu_n - \lambda_i - \varepsilon_{\Gamma_3})^{-1}$, where $\varepsilon_{\Gamma_3} = \varepsilon_{\Gamma_3}^{(0)} - 2\mu$, is unrenormalized. In the limit of $T \rightarrow 0$, Green functions, $F_{i\sigma}^{(0)}$, $B_{i\tau}^{(0)}$ and $G_{\mathbf{k}\tau\sigma}^{(0)}$ are given by

$$F_{i\sigma}^{(0)}(i\epsilon_n) = \frac{a}{i\epsilon_n - \lambda_i - (\varepsilon_{\Gamma_3} - E_0)} + C^{(0)}(i\epsilon_n), \quad (14)$$

$$B_{i\tau}^{(0)}(i\nu_n) = \frac{1}{i\nu_n - \lambda_i - \varepsilon_{\Gamma_3}}, \quad (15)$$

$$G_{\mathbf{k}\tau\sigma}^{(0)}(i\epsilon_n) = \frac{1}{i\epsilon_n - \xi_{\mathbf{k}} - \Sigma_{\mathbf{k}\tau\sigma}^{(0)}(i\epsilon_n)} \quad (16)$$

where a is the residue of the slave fermion, E_0 is the binding energy of the slave fermion relative to the chemical potential μ and corresponds to the Kondo temperature $T_K = D \exp(-1/|J|N_F)$ in the impurity Anderson model, where D is half the band width of the conduction electrons, J is the c - f exchange interaction, and N_F is the density of states of the conduction electrons. Hereafter, E_0 is used in theoretical expressions while T_K is used in figures which can be compared with experiments. The point is that E_0 and T_K are equivalent quantities. It is remarked that $(\varepsilon_{\Gamma_3} - E_0)$ in Eq. (14) is the effective level of f^1 -state renormalized by the self-energy of $O((1/N)^0)$. $\Sigma_{\mathbf{k}}^{(0)}(i\epsilon_n)$ in Eq. (16) is the self-energy of the conduction electrons of $O(1/N)$. Note that ϵ_n , in Eqs. (14) and (16), is the fermionic Matsubara frequency, $\epsilon_n = (2n+1)\pi T$, and ν_n , in Eq. (15), is the bosonic Matsubara frequency, $\nu_n = 2n\pi T$. $C^{(0)}(i\epsilon_n)$ in Eq. (14) represents the incoherent part of the slave fermion far from the Fermi level (or the chemical potential μ), and is given by

$$\begin{aligned} C^{(0)}(i\epsilon_n) = & a(i\epsilon_n - \lambda - \varepsilon_{\Gamma_3} + \varepsilon_{\Gamma_7} + E_0) \frac{V^2}{N_L} \sum_{\mathbf{k},\sigma} F_{i\sigma}^{(0)}(i\epsilon_n) \\ & \times \int d\epsilon f(\epsilon) \frac{-1}{\pi} \text{Im}G_{\mathbf{k}\tau\sigma}^{(0)}(\epsilon + i0_+) \frac{1}{(\epsilon - E_0)^2(i\epsilon_n + \epsilon - \lambda - \varepsilon_{\Gamma_3} + \varepsilon_{\Gamma_7})}, \end{aligned} \quad (17)$$

where $f(x)$ is the Fermi distribution function $f(x) \equiv 1/(e^{x/T} + 1)$. One can see from Eq. (17) that $\text{Im}C(\epsilon + i0_+)$ is non-zero only in the region $\epsilon \geq \varepsilon_{\Gamma_3} - \varepsilon_{\Gamma_7} + \lambda_i$. On the other hand, $\Sigma_{\mathbf{k}\tau\sigma}^{(0)}(i\epsilon_n)$ in Eq. (16) is given by

$$\begin{aligned} \Sigma_{\mathbf{k}\tau\sigma}^{(0)}(i\epsilon_n) \equiv & \frac{V^2}{N_L} \sum_i \lim_{\lambda_i \rightarrow \infty} \left[-T \sum_{\nu_n} F_{i\sigma}^{(0)}(i\epsilon_n + i\nu_n) \right. \\ & \left. \times B_{i\tau}^{(0)}(i\nu_n) / \langle \hat{Q}_i \rangle_{\lambda}^{(0)} \right], \end{aligned} \quad (18)$$

where $\langle \hat{Q}_i \rangle_{\lambda}^{(0)}$ denotes contributions of $O((1/N)^0)$ to $\langle \hat{Q}_i \rangle_{\lambda}$ in the $1/N$ -expansion:

$$\langle \hat{Q}_i \rangle_{\lambda}^{(0)} = M e^{-\beta(\lambda_i + \varepsilon_{\Gamma_3} - \varepsilon_{\Gamma_7} - E_0)}. \quad (19)$$

Then, the contribution of $\text{Im}C(\epsilon + i0_+)$ to $\Sigma_{\mathbf{k}\tau\sigma}^{(0)}(i\epsilon_n)$ is smaller than the imaginary part by a factor of $e^{-\beta E_0} \rightarrow 0$ (as $T \rightarrow 0$). Therefore, $\Sigma_{\mathbf{k}\tau\sigma}^{(0)}(i\epsilon_n)$ is approximately given by

$$\Sigma_{\mathbf{k}\tau\sigma}^{(0)}(i\epsilon_n) \simeq \frac{1}{M} \frac{aV^2}{i\epsilon_n - E_0}, \quad (20)$$

where E_0 and a are determined by solving the following coupled equations:

$$\varepsilon_{\Gamma_3} - \varepsilon_{\Gamma_7} - E_0 - \frac{V^2}{N_L} \sum_{\mathbf{k},\tau} \int d\epsilon f(\epsilon) \frac{-1}{\pi} \text{Im}G_{\mathbf{k}\tau\sigma}^{(0)}(\epsilon + i0_+) \frac{1}{\epsilon - E_0} = 0, \quad (21)$$

and

$$\frac{1}{a} = 1 + \frac{V^2}{N_L} \sum_{\mathbf{k},\tau} \int d\epsilon f(\epsilon) \frac{-1}{\pi} \text{Im}G_{\mathbf{k}\tau\sigma}^{(0)}(\epsilon + i0_+) \frac{1}{(\epsilon - E_0)^2}. \quad (22)$$

The residue a is approximately given by $a \simeq E_0/N_F V^2$, since the second term on the r.h.s. of Eq. (22) is approximately given by $N_F V^2/E_0$ if we note that the approximate relation $\frac{1}{N_L} \sum_{\mathbf{k}} (-1/\pi) \text{Im}G_{\mathbf{k}\tau\sigma}^{(0)}(\epsilon + i0_+) \simeq N_F$ holds. With the use of this self-energy, the Green function $G_{\mathbf{k}\tau\sigma}^{(0)}(i\epsilon_n)$ [Eq. (16)] for the conduction electron is expressed as follows:

$$G_{\mathbf{k}}^{(0)}(i\epsilon_n) = \sum_{\gamma=\pm} \frac{A_{\mathbf{k}}^{\gamma}}{i\epsilon_n - E_{\mathbf{k}}^{\gamma}}, \quad (23)$$

where

$$E_{\mathbf{k}}^{\gamma} = \frac{1}{2} \left[\varepsilon_{\mathbf{k}} + E_0 + \gamma \sqrt{(\varepsilon_{\mathbf{k}} - E_0)^2 + 4aV^2/M} \right], \quad (24)$$

and

$$A_{\mathbf{k}}^{\gamma} = \frac{E_{\mathbf{k}}^{\gamma} - E_0}{E_{\mathbf{k}}^{\gamma} - E_{\mathbf{k}}^{-\gamma}}. \quad (25)$$

Here we note that the self-energy of conduction electrons of $O((1/N)^0)$, $\Sigma_{\mathbf{k}\tau\sigma}^{(0)}(\epsilon + i0_+)$, does not have an imaginary part at $\epsilon = 0$ nor the incoherent part away from the Fermi level, so that only a quasiparticle band is formed and the system behaves as a Fermi liquid. In order to obtain those terms arising from incoherent contributions, we need to take into account contributions of $O(1/N)$, as discussed in subsections below.

2.3 Vertices of $O((1/N)^0)$

In order to calculate the the self-energy of $O(1/N)$ we need the full vertices up to $O((1/N)^0)$. The diagrams contributing to local vertices of $O((1/N)^0)$, are shown in Fig. 3(a), in which there is no summation with respect to the wave vectors.

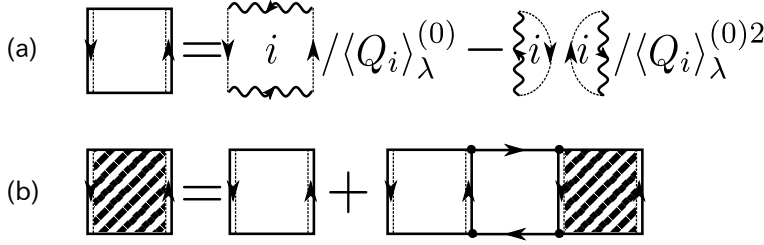


Fig. 3. (a) The local vertex $\Gamma^{\text{loc}(0)}$ of $O((1/N)^0)$, and (b) the full vertex $\Gamma_q^{(0)}$ of $O((1/N)^0)$.

$\Gamma^{\text{loc}(0)}(i\epsilon_{n1}, i\epsilon_{n2}; i\nu_n)$ denotes the sum of these contributions, which is given by

$$\begin{aligned} & \Gamma^{\text{loc}(0)}(i\epsilon_{n1}, i\epsilon_{n2}; i\nu_n) \\ &= \Gamma^{\text{loc}(0A)}(i\epsilon_{n1}, i\epsilon_{n2}; i\nu_n) + \Gamma^{\text{loc}(0B)}(i\epsilon_{n1}, i\epsilon_{n2}; i\nu_n), \end{aligned} \quad (26)$$

where the vertex $\Gamma^{\text{loc}(0A)}$ includes no singular term,

$$\begin{aligned} & \Gamma^{\text{loc}(0A)}(i\epsilon_{n1}, i\epsilon_{n2}; i\nu_n) \\ &= \frac{a^2 V^4}{M} \left[\frac{\bar{F}(-i\nu_n)}{(i\epsilon_{n1} - E_0)(i\epsilon_{n2} - E_0)} \right. \\ & \quad \left. + \frac{\bar{F}(i\nu_n)}{(i\epsilon_{n1} + i\nu_n - E_0)(i\epsilon_{n2} + i\nu_n - E_0)} \right] \delta_{\sigma_1, \sigma_4} \delta_{\sigma_2, \sigma_3}, \end{aligned} \quad (27)$$

where

$$\bar{F}(z) = \frac{1}{a} F_{i\sigma}^{(0)}(z + \lambda_i + \varepsilon_{\Gamma_3} - E_0), \quad (28)$$

while the vertex $\Gamma^{\text{loc}(0B)}$ includes a singular term proportional to T^{-1} ,

$$\begin{aligned} \Gamma^{\text{loc}(0B)}(i\epsilon_{n1}, i\epsilon_{n2}; i\nu_n) &= -\frac{a^2 V^4}{M} \frac{1}{T} \delta_{\nu_n} \frac{1}{(i\epsilon_{n1} - E_0)(i\epsilon_{n2} - E_0)} \\ & \times (\delta_{\sigma_1, \sigma_4} \delta_{\sigma_2, \sigma_3} - M^{-1} \delta_{\sigma_1, \sigma_3} \delta_{\sigma_2, \sigma_4}). \end{aligned} \quad (29)$$

$\Gamma^{\text{loc}(0B)}$ is zero in the single-channel case because $\sigma_1 = \sigma_2 = \sigma_3 = \sigma_4$ and $M = 1$.

The full vertex of $O((1/N)^0)$, which contributes to the imaginary part of the self-energy of conduction electrons, is defined by the Bethe-Salpeter equation illustrated in Fig. 3(b), because the number of the sum of wave vector and the number of the sum of τ are same in each diagram.

By denoting the full vertex of $O((1/N)^0)$ as $\Gamma_q^{(0)}(i\epsilon_{n1}, i\epsilon_{n2}; i\nu_n)$, we obtain

$$\begin{aligned} & \Gamma_q^{(0)}(i\epsilon_{n1}, i\epsilon_{n2}; i\nu_n) \\ &= \Gamma_q^{(0A)}(i\epsilon_{n1}, i\epsilon_{n2}; i\nu_n) + \Gamma_q^{(0B)}(i\epsilon_{n1}, i\epsilon_{n2}; i\nu_n), \end{aligned} \quad (30)$$

where $\Gamma_{\mathbf{q}}^{(0A)}$ makes contribution in both cases of single channel and multichannel, and has no singular term:

$$\begin{aligned}
& \Gamma_{\mathbf{q}}^{(0A)}(i\epsilon_{n1}, i\epsilon_{n2}; i\nu_n) \\
= & \delta_{\sigma_1, \sigma_4} \delta_{\sigma_2, \sigma_3} \frac{a^2 V^4}{M} \frac{1}{K_{\mathbf{q}}(i\nu_n)} \\
& \times \left\{ \frac{\bar{F}(i\nu_n)}{i\epsilon_{n1} + i\nu_n - E_0} \left[\frac{1 + \bar{F}(-i\nu_n) f_{\mathbf{q}}^{(0,2)}(i\nu_n)}{i\epsilon_{n2} + i\nu_n - E_0} - \frac{\bar{F}(-i\nu_n) f_{\mathbf{q}}^{(1,1)}(i\nu_n)}{i\epsilon_{n2} - E_0} \right] \right. \\
& \left. - \frac{\bar{F}(-i\nu_n)}{i\epsilon_{n1} - E_0} \left[\frac{\bar{F}(i\nu_n) f_{\mathbf{q}}^{(1,1)}(i\nu_n)}{i\epsilon_{n2} + i\nu_n - E_0} - \frac{1 + \bar{F}(i\nu_n) f_{\mathbf{q}}^{(2,0)}(i\nu_n)}{i\epsilon_{n2} - E_0} \right] \right\}, \quad (31)
\end{aligned}$$

while the vertex $\Gamma_{\mathbf{q}}^{(0B)}$ makes contribution only in the multichannel case and consists of a singular term:

$$\begin{aligned}
& \Gamma_{\mathbf{q}}^{(0B)}(i\epsilon_{n1}, i\epsilon_{n2}; i\nu_n) \\
= & -(\delta_{\sigma_1, \sigma_4} \delta_{\sigma_2, \sigma_3} - M^{-1} \delta_{\sigma_1, \sigma_3} \delta_{\sigma_2, \sigma_4}) \\
& \times \frac{a^2 V^4}{M} \frac{1}{T} \delta_{\nu_n} \frac{1}{K_{\mathbf{q}}(0) [K_{\mathbf{q}}(0) - T^{-1} f_{\mathbf{q}}^{(0,2)}(0)]} \\
& \times \frac{1}{i\epsilon_{n1} - E_0} \left[1 - f_{\mathbf{q}}^{(0,3)}(0) + \frac{f_{\mathbf{q}}^{(0,2)}(0)}{i\epsilon_{n1} - E_0} \right] \\
& \times \frac{1}{i\epsilon_{n2} - E_0} \left[1 - f_{\mathbf{q}}^{(0,3)}(0) + \frac{f_{\mathbf{q}}^{(0,2)}(0)}{i\epsilon_{n2} - E_0} \right], \quad (32)
\end{aligned}$$

where

$$\begin{aligned}
f_{\mathbf{q}}^{(l,m)}(i\nu_n) &= \frac{a^2 V^4}{M} T \sum_{\epsilon_n} \frac{1}{(i\epsilon_n + i\nu_n - E_0)^l (i\epsilon_n - E_0)^m} \\
&\times \frac{1}{N_L} \sum_{\sigma, \mathbf{k}} G_{\mathbf{k}+\mathbf{q}}(i\epsilon_n + i\nu_n) G_{\mathbf{k}}(i\epsilon_n), \\
& \quad (33)
\end{aligned}$$

$$\begin{aligned}
& K_{\mathbf{q}}(i\nu_n) \\
= & 1 + \bar{F}(-i\nu_n) f_{\mathbf{q}}^{(0,2)}(i\nu_n) + \bar{F}(i\nu_n) f_{\mathbf{q}}^{(2,0)}(i\nu_n) \\
& + \bar{F}(-i\nu_n) \bar{F}(i\nu_n) \left\{ f_{\mathbf{q}}^{(0,2)}(i\nu_n) f_{\mathbf{q}}^{(2,0)}(i\nu_n) - [f_{\mathbf{q}}^{(1,1)}(i\nu_n)]^2 \right\}. \\
& \quad (34)
\end{aligned}$$

Although the explicit expression of Eq. (34) is rather lengthy, $K_{\mathbf{q}}(0)$ is given by relatively

simple form as

$$\begin{aligned} K_{\mathbf{q}}(0) &= [1 - f_{\mathbf{q}}^{(0,3)}(0)]^2 - f_{\mathbf{q}}^{(0,2)}(0)f_{\mathbf{q}}^{(0,4)}(0) \\ &\quad + \frac{2}{a}C(\lambda + \varepsilon_{\Gamma_3} - \varepsilon_{\Gamma_7} - E_0)f_{\mathbf{q}}^{(0,2)}(0). \end{aligned} \quad (35)$$

Here, we note that the second term in the square bracket in the denominator in the r.h.s. of Eq. (32) includes a singular term which is proportional to T^{-1} . The details of the calculations of vertices $\Gamma^{\text{loc}(0)}$ and $\Gamma_{\mathbf{q}}^{(0)}$ are given in Sect. 3 of Ref. 11.

2.4 Self-energy of $O(1/N)$

Now, we calculate the self-energy of conduction electrons up to $O(1/N)$ in the two-channel case ($M = 2$) to prove that the imaginary part of the self-energy does not satisfy the Fermi liquid relation even though the system retains the translational symmetry. Let us denote the contribution, from the Feynman diagram shown by the l.h.s. of the diagrammatic relation in Fig. 4, as $\Delta\Sigma_{\mathbf{k}\tau\sigma}^{(1)}$ which is of the order of $O(1/N)$ according to the rule [Eq. (13)], because there is one summation of wave vector and no summation of τ , and the full vertex Γ depicted by striped square is of $O((1/N)^0)$ in the sense of $1/N$ -expansion formalism. Its non-zero imaginary part is given in the following form

$$\text{Im}\Delta\Sigma_{\mathbf{k}\tau\sigma}^{(1)}(\epsilon + i0_+) = \text{Im}\Delta\Sigma_{\mathbf{k}\tau\sigma}^{(1\text{FL})}(\epsilon + i0_+) + \text{Im}\Delta\Sigma_{\mathbf{k}\tau\sigma}^{(1\text{NFL})}(\epsilon + i0_+), \quad (36)$$

where $\text{Im}\Delta\Sigma_{\mathbf{k}\tau\sigma}^{(1\text{FL})}$ is the imaginary part of the self-energy of the Fermi liquid type:

$$\begin{aligned} &\text{Im}\Delta\Sigma_{\mathbf{k}\tau\sigma}^{(1\text{FL})}(\epsilon + i0_+) \\ &= -\pi \frac{1}{N_L^2} \sum_{\sigma, \mathbf{k}_1, \mathbf{k}_2} \sum_{\gamma_1, \gamma_2, \gamma_3} A_{\mathbf{k}_1}^{\gamma_1} A_{\mathbf{k}_2}^{\gamma_2} A_{\mathbf{k}-\mathbf{k}_1+\mathbf{k}_2}^{\gamma_3} \\ &\quad \times \left| \Gamma_{\mathbf{k}_2-\mathbf{k}_1}^{(0A)}(\epsilon, E_{\mathbf{k}_1}^{\gamma_1}; E_{\mathbf{k}_2}^{\gamma_2} - E_{\mathbf{k}_1}^{\gamma_1}) \right|^2 \\ &\quad \times \delta(\epsilon - E_{\mathbf{k}_1}^{\gamma_1} + E_{\mathbf{k}_2}^{\gamma_2} - E_{\mathbf{k}-\mathbf{k}_1+\mathbf{k}_2}^{\gamma_3}) \\ &\quad \times \frac{\cosh(\epsilon/2T)}{4 \cosh(E_{\mathbf{k}_1}^{\gamma_1}/2T) \cosh(E_{\mathbf{k}_2}^{\gamma_2}/2T) \cosh(E_{\mathbf{k}-\mathbf{k}_1+\mathbf{k}_2}^{\gamma_3}/2T)} \quad (37) \end{aligned}$$

$$\simeq -\pi\alpha_{\mathbf{k}}^{(1)} [\epsilon^2 + (\pi T)^2], \quad (38)$$

and $\text{Im}\Delta\Sigma_{\mathbf{k}\tau\sigma}^{(1\text{NFL})}$ is the imaginary part of the self-energy of the non-Fermi liquid type which does not appear in the single-channel case,

$$\begin{aligned} &\text{Im}\Delta\Sigma_{\mathbf{k}\tau\sigma}^{(1\text{NFL})}(\epsilon + i0_+) \\ &= -\pi \left(\frac{aV^2}{\epsilon - E_0} \right)^2 \frac{1}{N_L} \sum_{\mathbf{q}} \frac{\rho_{\mathbf{k}+\mathbf{q}}(\epsilon)}{K_{\mathbf{q}}(0) - T^{-1}f_{\mathbf{q}}^{(0,2)}(0)} \end{aligned}$$

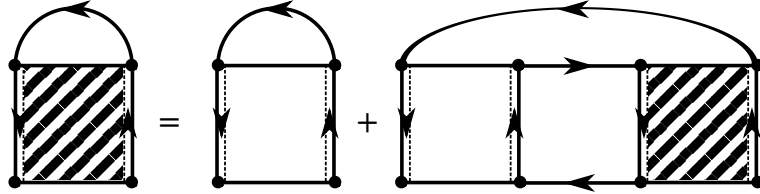


Fig. 4. Feynman-diagram representation of the self-energy $\Delta\Sigma_{\mathbf{k}\tau\sigma}^{(1)}(i\epsilon_n)$. This is based on that representing the Bethe-Salpeter equation for the full vertex Γ shown in Fig. 3(b). The striped square represents the full vertex Γ of $O((1/N)^0)$, which consists of the local part depicted by the open square, and the part giving the inter-site effect through the particle-hole propagation of conduction electrons.

$$\times \frac{1}{K_{\mathbf{q}}(0)} \left[1 - f_{\mathbf{q}}^{(0,3)}(0) + \frac{f_{\mathbf{q}}^{(0,2)}(0)}{\epsilon - E_0} \right]^2 \left(1 - \frac{1}{M^2} \right). \quad (39)$$

The coefficient $\alpha_{\mathbf{k}}^{(1)}$ in Eq. (38) is a constant of the order of $V^2 N_F / E_0^2$, and $\rho_{\mathbf{k}}(\epsilon)$ in Eq. (39) is the spectral function of conduction electrons,

$$\rho_{\mathbf{k}\tau\sigma}(\epsilon) = -\frac{1}{\pi} \text{Im} G_{\mathbf{k}\tau\sigma}(\epsilon + i0_+). \quad (40)$$

With the use of the Kramers-Krönig relation, the real part of the self-energy is calculated as follows:

$$\text{Re}\Sigma_{\mathbf{k}\tau\sigma}(\epsilon + i0_+) = \frac{1}{\pi} P \int \frac{\text{Im}\Sigma_{\mathbf{k}\tau\sigma}(\epsilon' + i0_+)}{\epsilon' - \epsilon} d\epsilon'. \quad (41)$$

There are other diagrams of $O(1/N)$ shown in Figs. 6 (a), (c)-(k) in Ref. 11 which contribute to the self-energy but they only modify E_0 and the chemical potential. Therefore, we neglect those diagrams. As a result, in the region $|\epsilon| \ll E_0$ and $T \ll E_0$, the self-energy of $O(1/N)$ is given as follows:

$$\begin{aligned} \Sigma_{\mathbf{k}\tau\sigma}(\epsilon + i0_+) &= \frac{1}{M} \frac{\tilde{a}_{\mathbf{k}} V^2}{\epsilon - \tilde{E}_{0\mathbf{k}}} - \Delta\mu_{\mathbf{k}}(\epsilon) \\ &\quad - \pi i \alpha_{\mathbf{k}}^{(1)} [\epsilon^2 + (\pi T)^2] - \pi i \frac{\beta_{\mathbf{k}}^{(1)}}{1 + T_{\mathbf{k}}^*/T} (1 - M^{-2}), \end{aligned} \quad (42)$$

where the imaginary part is the approximate expression with high accuracy of that given by Eq. (39), as verified numerically. Coefficients $\alpha_{\mathbf{k}}^{(1)}$ and $\beta_{\mathbf{k}}^{(1)}$ are proportional to $N_F V^2 T_K^{-2}$ and N_F^{-1} , respectively.

3. Chemical Potential

In this section, we discuss how the T dependence of the chemical potential $\mu(T)$ is calculated. To this end, we first determine the Green functions to the order of $O(1/N)$ by solving the Dyson equations shown diagrammatically in Fig. 5.

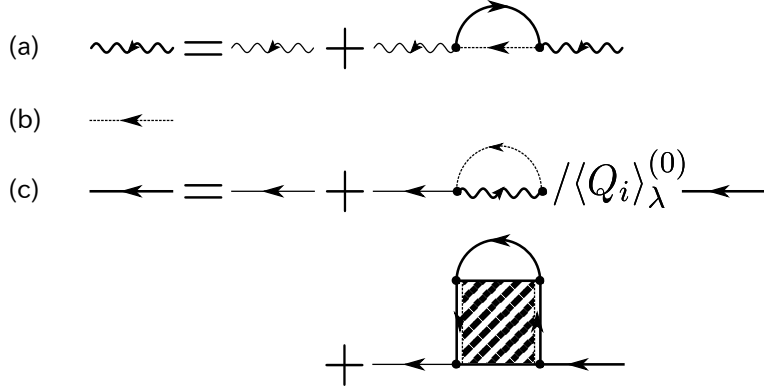


Fig. 5. Feynman diagram representation of the Dyson equations for the single-particle Green functions of the order of $O(1/N)$: (a) $F_{i\sigma}^{(1)}(i\epsilon_n)$ for the slave-fermion, (b) $B_{i\tau}^{(1)}(i\nu_n)$ for the pseudo boson, and (c) $G_{k\tau\sigma}^{(1)}(i\epsilon_n)$ for the conduction electron.

The T dependence of $\mu(T)$ is determined, by solving the following self-consistent equations

$$n_{tot} = n_c + n_f \quad (43)$$

$$n_c = \frac{1}{M} \sum_{\sigma=1}^M \sum_{\tau=1}^N \frac{1}{N_L} \sum_{\mathbf{k}} \int_{-\infty}^{\infty} d\epsilon \left[-\frac{1}{\pi} \text{Im}G_{\mathbf{k}\tau\sigma}^{(1)}(\epsilon + i0_+) \right] f(\epsilon) \quad (44)$$

$$n_f = (2n_{\text{pseudo boson}} + n_{\text{slave fermion}})/2, \quad (45)$$

where n_{tot} is the total electron number per site and per channel, n_c is the conduction electron number per site and per channel, $n_{\text{pseudo boson}}$ is the number of the pseudo boson per site, $n_{\text{slave fermion}}$ is the number of the slave fermion per site, and n_f is the f -electron number per site and per channel, and is given by

$$n_f = 1 - \frac{a}{2}. \quad (46)$$

In deriving Eq. (46) from Eq. (45), we have used the relations, $n_{\text{pseudo boson}} = 1 - a$, and $n_{\text{slave fermion}} = a$. Now, instead of Eqs. (21) and (22), residue a and the binding energy E_0 of the slave fermion should be determined to the order of $O(1/N)$ by solving coupled self-consistent equations

$$\varepsilon_{\Gamma_3} - \varepsilon_{\Gamma_7} - E_0 - \frac{V^2}{N_L} \sum_{\mathbf{k},\tau} \int d\epsilon f(\epsilon) \frac{-1}{\pi} \text{Im}G_{\mathbf{k}\tau\sigma}^{(1)}(\epsilon + i0_+) \frac{1}{\epsilon - E_0} = 0, \quad (47)$$

and

$$\frac{1}{a} = 1 + \frac{V^2}{N_L} \sum_{\mathbf{k},\tau} \int d\epsilon f(\epsilon) \frac{-1}{\pi} \text{Im}G_{\mathbf{k}\tau\sigma}^{(1)}(\epsilon + i0_+) \frac{1}{(\epsilon - E_0)^2}, \quad (48)$$

where the retarded Green function of conduction electrons is given by

$$G_{\mathbf{k}\tau\sigma}^{(1)}(\epsilon + i0_+) = \frac{1}{\epsilon + i0_+ - \xi_{\mathbf{k}} - \Sigma_{\mathbf{k}\tau\sigma}(\epsilon + i0_+)}, \quad (49)$$

with the retarded self-energy given by

$$\Sigma_{\mathbf{k}\tau\sigma}(\epsilon + i0_+) = \Sigma_{\mathbf{k}\tau\sigma}^{(0)}(\epsilon + i0_+) + \Delta\Sigma_{\mathbf{k}\tau\sigma}^{(1)}(\epsilon + i0_+), \quad (50)$$

where $\Sigma_{\mathbf{k}\tau\sigma}^{(0)}(\epsilon + i0_+)$ and $\Delta\Sigma_{\mathbf{k}\tau\sigma}^{(1)}(\epsilon + i0_+)$ are self-energies given by Eqs. (20) and (36)-(39), respectively. The Green function for the slave fermion of the order of $O(1/N)$, $F_{i\sigma}^{(1)}$, is given by

$$F_{i\sigma}^{(1)}(i\epsilon_n) = \frac{a}{i\epsilon_n - \lambda_i - (\varepsilon_{\Gamma_3} - E_0)} + C^{(1)}(i\epsilon_n), \quad (51)$$

$$(52)$$

where

$$\begin{aligned} C^{(1)}(i\epsilon_n) &= a(i\epsilon_n - \lambda - \varepsilon_{\Gamma_3} + \varepsilon_{\Gamma_7} + E_0) \frac{V^2}{N_L} \sum_{\mathbf{k},\sigma} F_{i\sigma}^{(1)}(i\epsilon_n) \\ &\times \int d\epsilon f(\epsilon) \frac{-1}{\pi} \text{Im}G_{\mathbf{k}\tau\sigma}^{(1)}(\epsilon + i0_+) \frac{1}{(\epsilon - E_0)^2(i\epsilon_n + \epsilon - \lambda - \varepsilon_{\Gamma_3} + \varepsilon_{\Gamma_7})}. \end{aligned} \quad (53)$$

The relation $a \simeq E_0/N_F V^2$ obtained to the order of $O((1/N)^0)$ is not seriously altered even to the order of $O(1/N)$, which we have verified by numerical calculations.

In numerical calculations below, we use the constant density of states $N(\epsilon)$ for conduction electrons given by

$$N(\epsilon) = \begin{cases} \frac{1}{D} & (|\epsilon| \leq D) \\ 0 & (\text{otherwise}), \end{cases} \quad (54)$$

with parameters chosen as the total electron number $n_{tot} = 2.0$, $D = 1$, $V = 0.3$, $\varepsilon_{\Gamma_3}^{(0)} - \varepsilon_{\Gamma_7}^{(0)} = -0.5$, $M = 2$ and $N = 2$, which lead to $E_0 = 0.0607$, $a = 0.437$, $\mu = -0.332$ and the effective mass of the quasi-particle $m^*/m = 6.35$. Hereafter, we use this parameters set, unless otherwise stated.

Figure 6 shows the spectral weight of conduction electrons, $\rho_{\mathbf{k}\tau\sigma}(\epsilon)$, defined by Eq. (40), at $T = 0$. At the Fermi level, the effective mass is heavy, and the peak is very sharp. The localized state of conduction electrons at $\epsilon = \varepsilon_{\Gamma_3} - \varepsilon_{\Gamma_7} = -0.168D$ gives the spectral weight of conduction electrons a broad peak.

By numerically solving self-consistent equations [Eqs. (43)-(50)], the chemical potential μ is determined as a function of T and n . Figure 7(a) shows the T dependence

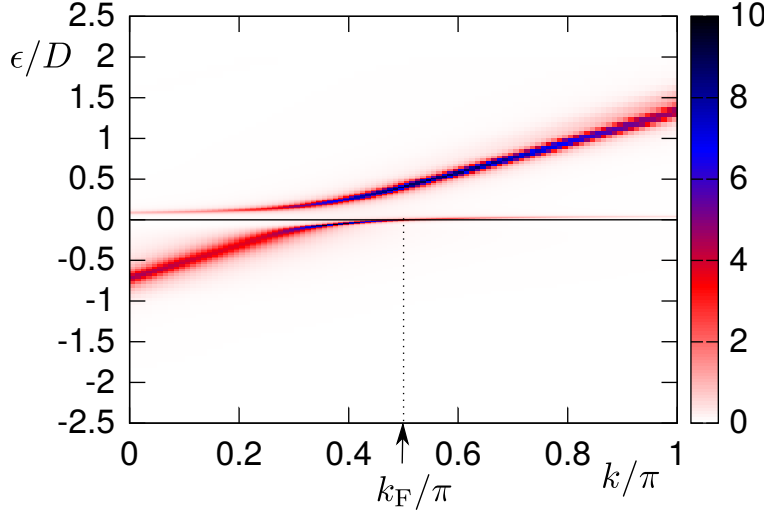


Fig. 6. The spectral weight $\rho_{k\tau\sigma}(\epsilon)D = -\text{Im}G_{k\tau\sigma}^{(1)}(\epsilon + i0_+)D/\pi$ in the unit of $1/D$ at $T = 0$ in $\epsilon\text{-}k$ plane. The Fermi wave number k_F is given by $k_F/\pi = 0.5$.

of $\mu(T)$. We note that the T dependence of $\mu(T)$ can be well fitted by the functional form as

$$\mu = \mu_0 \left(1 - a_4 \sqrt{T/E_0} \right), \quad (55)$$

in wide temperature region $T_x < T \ll T_K$, where T_x is a crossover temperature of the order of $0.0008T_K$. This should be compared with that in the case of single channel, where the so-called Fermi liquid (FL) behavior is obtained for $\mu(T)$ at $T \ll T_K$ without any crossover temperature scale other than T_K :

$$\mu = \mu_0 [1 - a_3(T/E_0)^2]. \quad (56)$$

as shown in Fig. 7(b). The origin of the non-Fermi liquid (NFL) behavior in $\mu(T)$ [Eq. (55)] can be traced back to the NFL ϵ - and T -dependence of the self-energy [Eq. (39)].

Through this anomalous T dependence of the chemical potential $\mu(T)$, various physical quantities turn out to have the anomalous NFL T dependence as shown in the following sections.

4. Resistivity

In this section, the T dependence of the electrical resistivity $\rho(T)$ is discussed. Although the conductivity (inverse of the resistivity) is, precisely speaking, given by the current-current response function consisting of fully renormalized Green function of conduction electrons and vertex corrections, we here adopt a simple approximation that the electrical resistivity ρ is proportional to the imaginary part of the self-energy

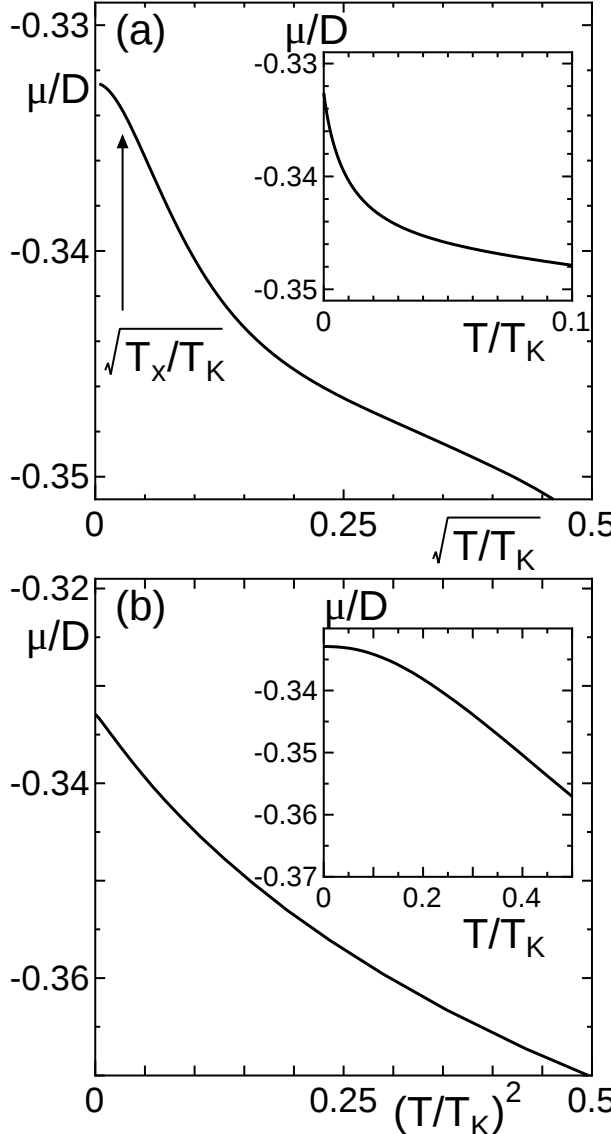


Fig. 7. (a) T dependence of the chemical potential $\mu(T)$ in the case of two channel, and (b) the case of single channel. T_x denotes the crossover temperature at which T dependence of $\mu(T)$ changes from $\propto T$ to $\propto \sqrt{T}$ as T increases.

$\Sigma_{\mathbf{k}\tau\sigma}(i0_+; T)$ of conduction electrons at the Fermi wave vector, because we are interested in qualitative properties and general aspects of the two-channel Anderson lattice model. Then, $\rho(T)$ is given as follows:

$$\rho = \rho_{\text{FL}} + \rho_{\text{NFL}}, \quad (57)$$

where ρ_{FL} stems from the FL type self-energy given by Eq. (38), and ρ_{NFL} from the NFL type self-energy given by Eq. (39). Explicit expressions for ρ_{FL} and ρ_{NFL} are

$$\rho_{\text{FL}} \simeq r \pi N_{\text{F}} V^2 \frac{T^2}{E_0^2}, \quad (58)$$

and

$$\begin{aligned} \rho_{\text{NFL}} \simeq & r \frac{a^2 V^4}{E_0^2 N_L} \sum_{\mathbf{q}} \frac{\rho_{\mathbf{k}+\mathbf{q}}(0)}{K_{\mathbf{q}}(0) - T^{-1} f_{\mathbf{q}}^{(0,2)}(0)} \\ & \times \frac{1}{K_{\mathbf{q}}(0)} \left[1 - f_{\mathbf{q}}^{(0,3)}(0) - \frac{f_{\mathbf{q}}^{(0,2)}(0)}{E_0} \right]^2 \left(1 - \frac{1}{M^2} \right) \Big|_{k=k_F}, \end{aligned} \quad (59)$$

where r is a ratio of the resistivity ρ and $-\text{Im}\Sigma_{k_F}(i0_+, T)$, which is the scattering rate of quasiparticles divided by mass renormalization amplitude, and is reduced to m/ne^2 in the case of an isotropic Fermi liquid.

Figure 8 shows the temperature dependence of ρ_{NFL} calculated from Eq. (59) for conduction electrons for the same parameters set mentioned above. In the low T region, $T < T_x \simeq 0.00076 T_K$, the resistivity is proportional to T as shown in Eq. (59), while \sqrt{T} dependence can be seen in $\text{Im}\Sigma_{k_F}(i0_+, T)$ in the region $0.00076 \leq T/T_K \leq 0.012$. Recently Sakai *et al.* and Onimaru *et al.* experimentally found \sqrt{T} dependence of the electrical resistivity in $\text{PrV}_2\text{Al}_{20}$ ¹⁾ and $\text{PrIr}_2\text{Zn}_{20}$,²⁾ respectively, in rather wide temperature region above the quadrupolar ordering temperature T_Q . We can fit our theoretical result to experimental one in Ref. 2, as demonstrated in Fig. 9 in which the theoretical results for ρ_{NFL} in the cases of (a) $V/D = 0.21$ and (b) $V/D = 0.25$ are shown. The Kondo temperatures T_K 's in these cases are $T_K/D \simeq 0.0197$ and $T_K/D \simeq 0.0351$, respectively, if other parameters are fixed as the same values adopted above. In order to obtain the best fit for these cases, we have to adjust D , half the band width of conduction electrons, and the factor r , parameterizing the ratio of the resistivity and $-\text{Im}\Sigma_{k_F}(0, T)$: i.e., $D = 1220\text{K}$ ($T_K = 24\text{K}$) and $rD = 6.67\mu\Omega\text{cm}$ in the case of (a), and $D = 540\text{K}$ ($T_K = 19\text{K}$) and $rD = 8.20\mu\Omega\text{cm}$ in the case of (b), respectively.

We can qualitatively understand this behavior as seen in Fig. 10. The imaginary part of the self-energy of conduction electrons, $-\text{Im}\Sigma(i0_+, T)$, is proportional to $-\log T$ in high temperature region $T \gtrsim T_K$ and there appears a peak at $T = T_{\text{max}}$, because the imaginary part has to be zero at $T = 0\text{K}$ in the lattice systems. In the case of two-channel, the second derivative is zero in the limit of $T \rightarrow 0$. Therefore, the second derivative is negative between $T = 0\text{K}$ and $T = T_{\text{max}}$. This negative second derivative

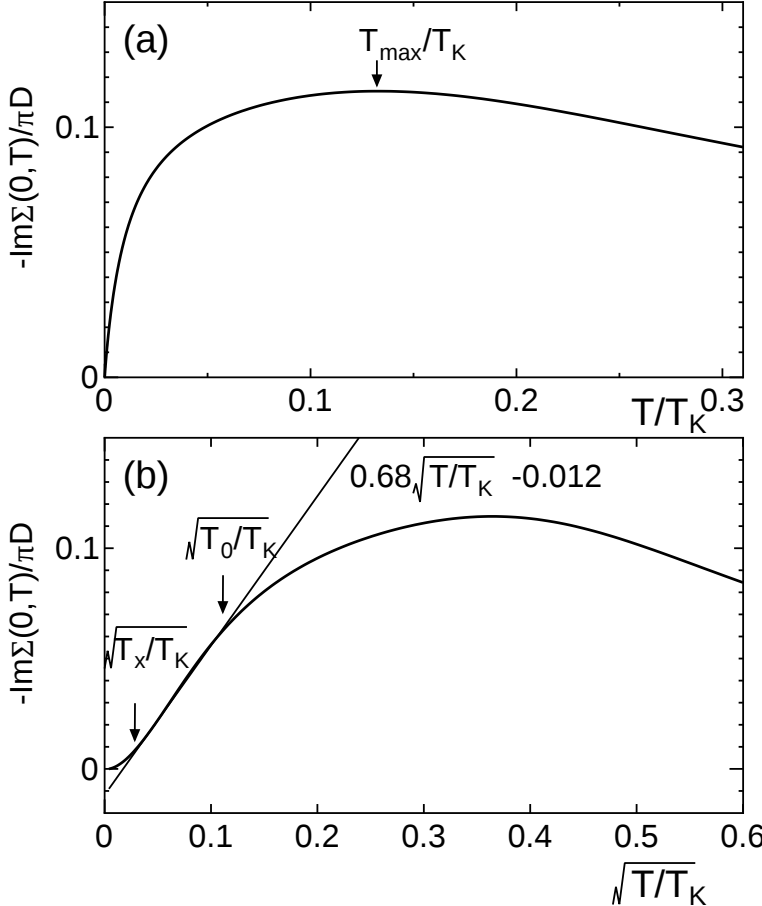


Fig. 8. (a) T/T_K dependence of $-\text{Im}\Delta\Sigma_{k_F\tau\sigma}^{(1)}(i0_+, T)/\pi D$, and (b) $\sqrt{T/T_K}$ dependence of $-\text{Im}\Delta\Sigma_{k_F\tau\sigma}^{(1)}(i0_+, T)/\pi D$. T_{\max} denotes the temperature at which $-\text{Im}\Sigma(0, T)$ takes maximum value. T_0 denotes the crossover temperature at which T dependence of $-\text{Im}\Sigma(0, T)$ deviates from the \sqrt{T} dependence to that with much lower exponent as T increases. T_x denotes the crossover temperature at which T dependence of $-\text{Im}\Sigma(0, T)$ changes from $\propto T$ to $\propto \sqrt{T}$ as T increases.

curve gives $-\text{Im}\Sigma_{\mathbf{k}\tau\sigma}(\epsilon = 0, T)$ an approximate \sqrt{T} dependence at $T < T_K$. On the other hand, in the case of single channel, it is proportional to T^2 in the limit of $T \rightarrow 0$. Around the peak, the second derivative of $-\text{Im}\Sigma_{\mathbf{k}\tau\sigma}(i0_+, T)$ is negative and it is positive near zero temperature. Therefore, in the middle region of T , the quantity $-\text{Im}\Sigma_{\mathbf{k}\tau\sigma}(i0_+, T)$ exhibits an approximate T -linear dependence.

Figure 11(a) shows the T dependence of the resistivity for a series of hybridization V 's. For larger V , the slope, in the limit $T \rightarrow 0$, becomes smaller. Figure 11(b) shows T/T_0 dependence of ρ_{NFL} , where T_0 is defined as the crossover temperature at which T dependence of ρ_{NFL} deviates from the \sqrt{T} dependence to that with much lower exponent as T increases, as shown in Fig. 11(c). This implies that $\rho(T)$'s for the systems with

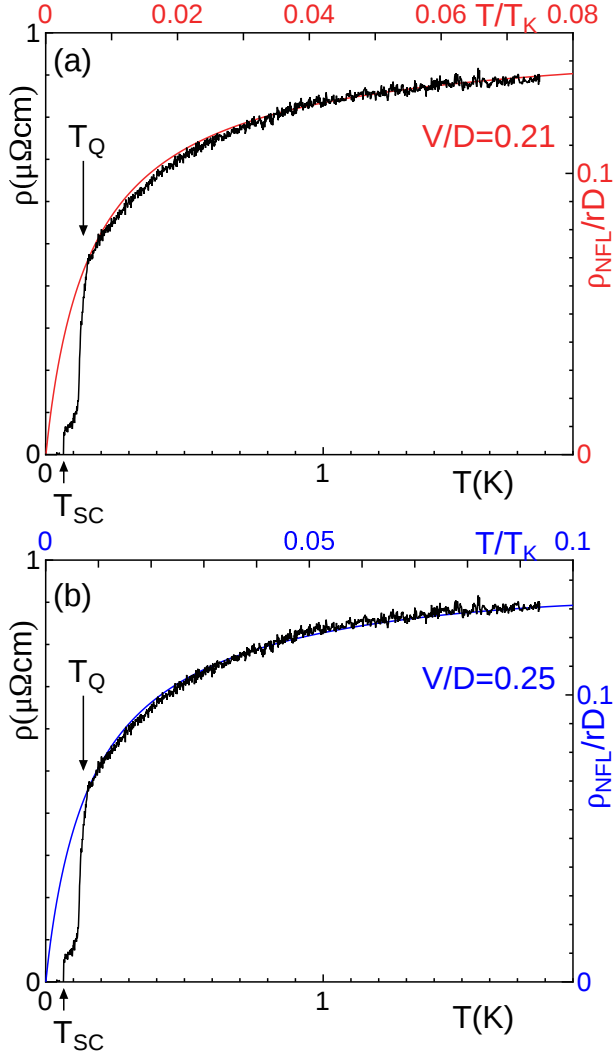


Fig. 9. Comparison of $\rho(T)$ (black jagged curves) observed in $\text{PrIr}_2\text{Zn}_{20}$ ²⁾ and theoretical results for $\rho_{\text{NFL}}(T)$ in the case of (a) $V/D = 0.21$ (red line) and (b) $V/D = 0.25$ (blue line) given by Eq. (59). T_Q and T_{SC} indicate the transition temperature for quadrupole ordering and superconducting ordering of $\text{PrIr}_2\text{Zn}_{20}$,²⁾ respectively. Note that the fundamental energy scale T_K is chosen as (a) $T_K = 24\text{K}$ and (b) $T_K = 19\text{K}$, the ratio of the resistivity r is chosen as (a) $rD = 6.67\mu\Omega\text{cm}$ and (b) $rD = 8.20\mu\Omega\text{cm}$, and the band width D is chosen as (a) $D = 1220\text{K}$ and (b) $D = 540\text{K}$.

different V 's fit in with a single curve if T is scaled by T_0 which is V dependent, as shown in Fig. 11(c). Namely, we obtain a scaling behavior $\rho(T) = R(T/T_0)$ with a single function $R(x)$ for different T_0 's. This scaling behavior in $\rho(T)$ has recently been observed in $\text{PrIr}_2\text{Zn}_{20}$ ²⁰⁾ and $\text{PrV}_2\text{Al}_{20}$ ²¹⁾ under pressure, and also in $\text{PrIr}_2\text{Zn}_{20}$ under magnetic field.²²⁾ As we show in Sect. 6, this kind of scaling behavior also holds in the T dependence of the specific heat $C(T)$, which is consistent with experimental finding in $\text{PrIr}_2\text{Zn}_{20}$.²⁰⁾

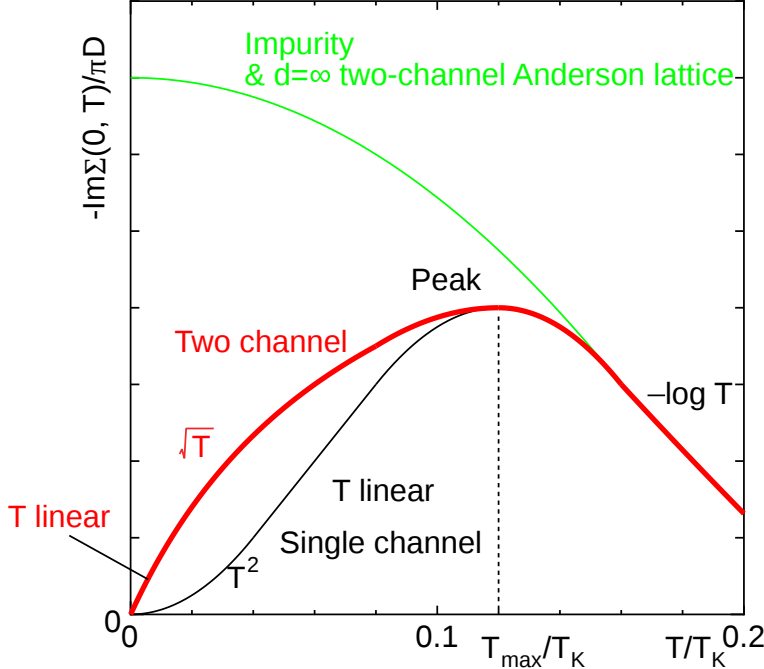


Fig. 10. Schematic T dependence of the $-\text{Im}\Sigma(i0_+, T)$, in arbitrary unit, in the case of single-channel Anderson lattice (black line), and impurity Anderson model and two-channel Anderson lattice in $d \rightarrow \infty$ (green line), and two channel Anderson lattice (red line). Note that $d^2\rho/dT^2 < 0$ at $T < T_{\text{max}}$ in the two-channel case, while $d^2\rho/dT^2 > 0$ at $T \ll T_{\text{max}}$ in the single-channel case.

According to Eqs. (57)-(59), we can rewrite the electrical resistivity at $T \lesssim T_{\text{max}} \ll E_0$ as

$$\rho = c_1 \frac{T^2}{E_0^2} + \frac{c_2}{1 + b \frac{E_0}{T}}, \quad (60)$$

where the coefficients c_1 and c_2 are given by $c_1 \simeq r\pi N_F V^2$ and $c_2 \simeq r(aV^2/E_0)^2 N_F \simeq r/N_F$. Here, we note that T_K is the same quantity as E_0 , as mentioned above. The coefficient b in the denominator of the second term of Eq. (60) is estimated as $b \simeq 1/(1 + N_F E_0)$ because $K_{\mathbf{q}}(0)$ and $f_{\mathbf{q}}^{(0,2)}(0)$ in the denominator of Eq. (59) are estimated as $K_{\mathbf{q}}(0) \simeq 1 + (1/N_F E_0)$ and $f_{\mathbf{q}}^{(0,2)}(0) \simeq 1/N_F$. Since $c_1 \simeq \pi(N_F V)^2 c_2$ and $N_F V$ is moderately smaller than 1 for heavy fermion systems, the NFL-type contribution, the second term of Eq. (60) dominates the FL-type one, the first term of Eq. (60) in the temperature region $T < T_{\text{max}} \ll E_0$.

Therefore, if $T_Q \ll T_{\text{max}}$, the NFL-type T dependence dominates the FL-type one at $T < T_{\text{max}}$, as observed in $\text{PrV}_2\text{Al}_{20}$ and $\text{PrIr}_2\text{Zn}_{20}$. On the other hand, if $T_Q \sim T_{\text{max}}$, the FL-type T dependence dominates the NFL-type one at $T > T_{\text{max}} \sim T_Q$, as observed in $\text{PrTi}_2\text{Al}_{20}$. Since the hybridization V of $\text{PrTi}_2\text{Al}_{20}$ is smaller than that of $\text{PrV}_2\text{Al}_{20}$,

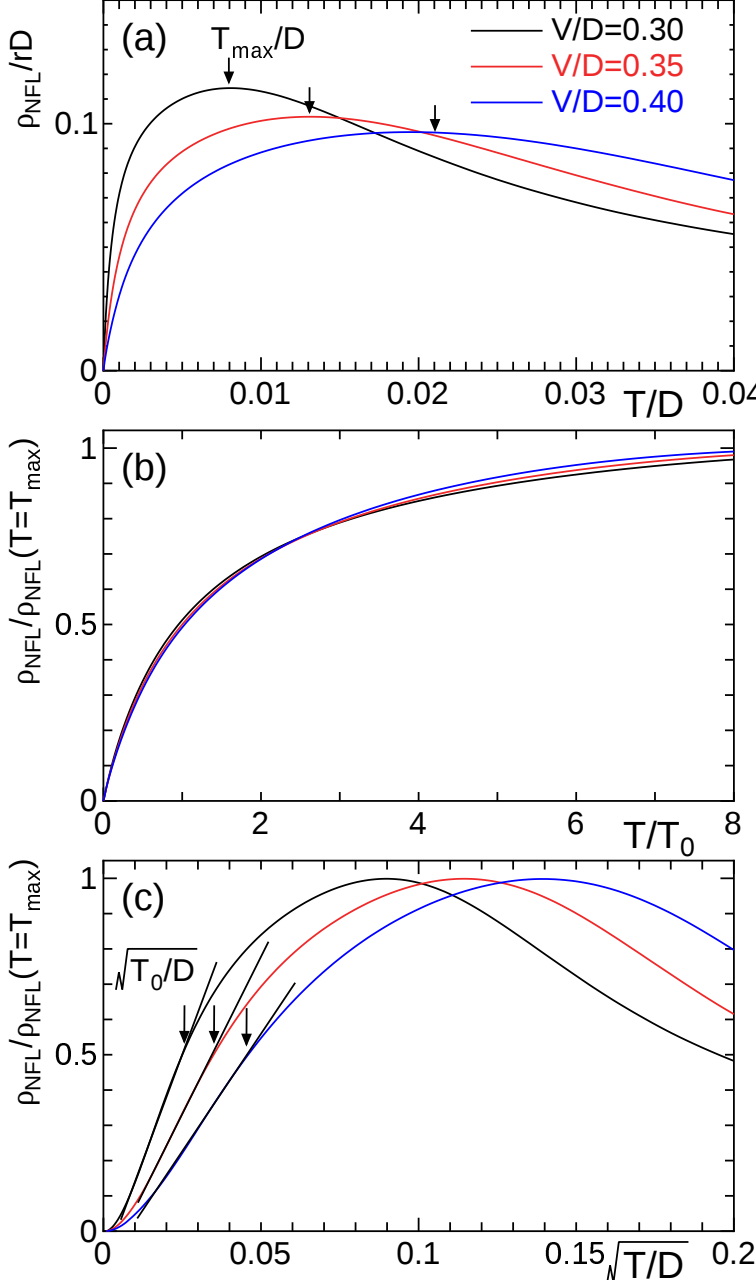


Fig. 11. (a) T/D dependence of ρ_{NFL} , defining T_{max} at which ρ_{NFL} takes maximum value, as shown by down arrow. (b) T/T_0 dependence of $\rho_{\text{NFL}}/\rho_{\text{NFL}}(T = T_{\text{max}})$ exhibiting an approximate scaling behavior. (c) Definition of T_0 (shown by down arrow) where T dependence of ρ_{NFL} , crossover from the \sqrt{T} dependence to that with much lower exponent as T increases.

the sister compound of $\text{PrV}_2\text{Al}_{20}$,¹⁾ T_Q of $\text{PrTi}_2\text{Al}_{20}$ is about three times higher than that of $\text{PrV}_2\text{Al}_{20}$, i.e., $T_Q^{\text{Ti}} \simeq 2\text{K}$ and $T_Q^V \simeq 0.6\text{K}$, and E_0 of $\text{PrTi}_2\text{Al}_{20}$ is expected to be far smaller than that of $\text{PrV}_2\text{Al}_{20}$ because E_0 has the sharp dependence on V as $E_0 \propto \exp(-|\varepsilon_{\Gamma_3} - \varepsilon_{\Gamma_7}|/V^2 N_F)$. Therefore, $(T_Q^{\text{Ti}}/E_0^{\text{Ti}})$ is expected to be far larger

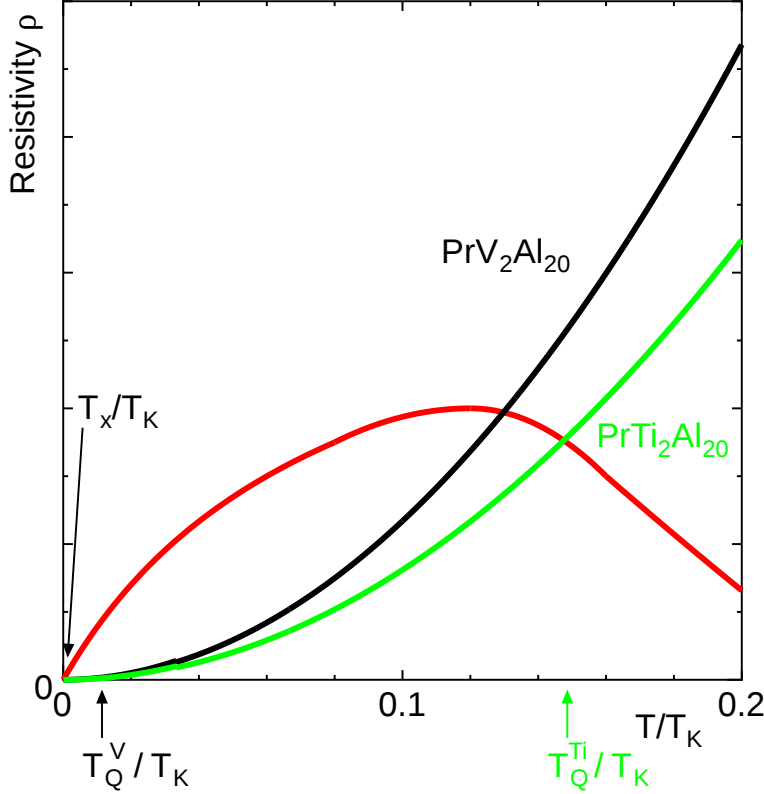


Fig. 12. Schematic T dependence of NFL and FL contributions to the resistivity for $\text{PrV}_2\text{Al}_{20}$ and $\text{PrTi}_2\text{Al}_{20}$. Red line indicates the NFL contribution shown in Fig. 10, and black and green lines are indicate the FL contributions for $\text{PrV}_2\text{Al}_{20}$ and $\text{PrTi}_2\text{Al}_{20}$, respectively.

than (T_Q^V/E_0^V) . This situation is shown in Fig. 12, explaining the fact that the FL-type T dependence in $\rho(T)$ is observed at $T > T_Q$ in $\text{PrTi}_2\text{Al}_{20}$, the sister compound of $\text{PrV}_2\text{Al}_{20}$ that exhibits the NFL-type T dependence in $\rho(T)$ at $T > T_Q$, as discussed above.

5. Difficulty of DMFT for Multichannel Anderson Lattice Model

In this section, the difficulty of the dynamical mean field theory (DMFT) when it is applied to calculating transport properties of the two-channel Anderson or Kondo lattice model is discussed.

The DMFT is known to give a correct T dependence of the resistivity $\rho(T)$ in the single-channel Anderson lattice model: $\rho(T) \propto T^2$ at $T \ll T_K$. On the other hand, it gives unphysical result in the two-channel Anderson or Kondo lattice model: $\rho(T) \propto \text{const.}$ in the limit $T \rightarrow 0$. Indeed, when the DMFT is applied to the two-channel Kondo lattice model with solvers of impurity problem such as the quantum Monte Carlo method¹⁶⁾ and the continuous-time quantum Monte Carlo method,²³⁾ the resistivity is

shown to be finite at even $T = 0$. However, in lattice systems that retain translational symmetry, the resistivity must be zero at $T = 0$ owing to the conservation law of lattice momentum.²⁴⁾ Such an insufficiency stems from the fact that the DMFT fails to take properly into account inter-site effects.

This situation can be explicitly analyzed on the formalism of the present paper. Those results suggest that the DMFT is not sufficient for including the inter-site effect. Indeed, if we take the limit of the infinite spatial dimension, i.e., $d \rightarrow \infty$, of terms giving for the self-energy $\Delta\Sigma_{\mathbf{k}\tau\sigma}^{(1NFL)}(\epsilon)$ [Eq. (39)], the second term on the r.h.s. of Fig. 4 (which manifests the inter-site effects through the particle-hole propagation of the conduction electrons) vanishes. This is because such a term including n local vertices Γ_{loc} 's, indicated by the open square, is of $O(d^{-(n-1)})$. Indeed, a factor V^4 appears through the hybridization between the conduction electrons and the local vertex Γ_{loc} and the wave vector summation of the particle-hole pair gives a factor d . Then, considering $V = O(1/\sqrt{d})$ in the limit $d \rightarrow \infty$, the term in question is estimated as follows:

$$(V^4\Gamma_{\text{loc}}d)^{n-1}\Gamma_{\text{loc}} \sim (d^{-2} \cdot d)^{n-1}(\Gamma_{\text{loc}})^n = d^{-(n-1)}(\Gamma_{\text{loc}})^n. \quad (61)$$

Therefore, the contribution from the second term on the r.h.s. of Fig. 4 can be neglected in the limit $d \rightarrow \infty$. On the other hand, the first term on the r.h.s. of Fig. 4 (which includes only the local vertex Γ_{loc} , and manifests the local and the on-site effect) remains non-vanishing even in the limit $d \rightarrow \infty$.

More explicitly, each quantity included in the r.h.s. of Eq. (39) is estimated as in the following arguments. According to the definition, Eq. (39), the property $V = O(1/d)$, and the fact that $(1/N_L)\sum_{\mathbf{k}}$ gives a factor proportional to the space dimension d , $f_{\mathbf{q}}^{(l,m)}(0)$'s given by Eq. (33) are estimated as

$$f_{\mathbf{q}}^{(0,2)}(0) = f_{\mathbf{q}}^{(2,0)}(0) \sim \frac{a^2 V^4}{E_0^2} \frac{N_F d}{a} \frac{a^2}{a} \propto \frac{d^{-1}}{N_F}, \quad (62)$$

$$f_{\mathbf{q}}^{(0,3)}(0) \sim \frac{a^2 V^4}{E_0^3} \frac{N_F d}{a} \frac{a^2}{a} \propto \frac{d^{-1}}{E_0 N_F}, \quad (63)$$

and

$$f_{\mathbf{q}}^{(1,1)}(0) \sim \frac{a^2 V^4}{E_0^2} \frac{N_F d}{a} \frac{a}{a} \propto \frac{d^{-1}}{N_F}, \quad (64)$$

$$(65)$$

where we have used the relation $aV^2N_Fd \sim E_0$. According to Eq. (17), d dependence

of $C(\lambda + \varepsilon_{\Gamma_3} - \varepsilon_{\Gamma_7} - E_0)$ is estimated as

$$C(\lambda + \varepsilon_{\Gamma_3} - \varepsilon_{\Gamma_7} - E_0) \sim aV^2 dN_F \frac{a}{E_0^2} \propto \frac{d^0 a}{E_0}. \quad (66)$$

Then, with the use of Eqs. (62)-(66), $K_q(0)$ defined by Eq. (35) is estimated in the limit $d \rightarrow \infty$ as

$$K_q(0) = 1 + O(d^{-1}). \quad (67)$$

Therefore, in the limit $d \rightarrow \infty$, $\text{Im}\Delta\Sigma_{\mathbf{k}\tau\sigma}^{(1\text{NFL})}(\epsilon + i0_+)$ [Eq. (39)] is given as follows:

$$\text{Im}\Delta\Sigma_{\mathbf{k}\tau\sigma}^{(1\text{NFL})}(\epsilon) = -\pi \left(\frac{aV^2}{\epsilon - E_0} \right)^2 \frac{1}{N_L} \sum_{\mathbf{k}} \rho_{\mathbf{k}\tau\sigma}(\epsilon) (1 - M^{-2}). \quad (68)$$

A crucial point of the estimation above is that, in the limit $d \rightarrow \infty$, $T^{-1}f_q^{(0,2)}(0)$ is neglected compared with $K_q(0)$ in the denominator in the first line on the r.h.s. of Eq. (39).

It is apparent that $\text{Im}\Delta\Sigma_{\mathbf{k}\tau\sigma}^{(1)}$ given by Eq. (68) remains finite even in the limit $T \rightarrow 0$. The above analysis, on the basis of $1/N$ -expansion approach, explicitly unveils the difficulty with results for the $\rho(T)$ obtained by using the DMFT. This shows that the inter-site effect is important to obtain correct results in the two-channel Anderson or Kondo lattice model, and that the DMFT is not valid at least for discussing transport properties. On the other hand, in the case of the single-channel ($M = 1$) model, $\text{Im}\Sigma_{\mathbf{k}\tau\sigma}^{(1\text{NFL})}(\epsilon)$ given by Eq. (39) identically vanishes irrespective of T so that the unphysical result does not appear, which is accidental.

6. Specific Heat

Under usual experimental condition, the specific heat is measured with fixed pressure P not with fixed volume V . On the other hand, it is the specific heat with fixed chemical potential μ and V that is easily calculated by the conventional many-body theory based on the field theoretical method with Feynman diagrams. Among these two specific heats, C_P (with fixed P) and C_V (with fixed V), the following relation holds:

$$C_P = T \left(\frac{\partial S}{\partial T} \right)_P = T \left(\frac{\partial S}{\partial T} \right)_V \frac{\left(\frac{\partial P}{\partial V} \right)_S}{\left(\frac{\partial P}{\partial V} \right)_T} = C_V \frac{\left(\frac{\partial P}{\partial V} \right)_S}{\left(\frac{\partial P}{\partial V} \right)_T}, \quad (69)$$

where C_V is given by Eq. (A-1) in Appendix A.

With the use of the relations of thermodynamic derivatives, the derivative $(\partial P/\partial V)_S$ in Eq. (65) is transformed as follows:

$$\left(\frac{\partial P}{\partial V} \right)_S = \frac{\partial(P, S)}{\partial(V, S)} = \frac{\partial(P, S)}{\partial(V, T)} \frac{\partial(V, T)}{\partial(V, S)}$$

$$\begin{aligned}
&= \left[\left(\frac{\partial P}{\partial V} \right)_T \left(\frac{\partial S}{\partial T} \right)_V - \left(\frac{\partial P}{\partial T} \right)_V \left(\frac{\partial S}{\partial V} \right)_T \right] \frac{1}{(\frac{\partial S}{\partial T})_V} \\
&= \left(\frac{\partial P}{\partial V} \right)_T \left[1 - \frac{(\frac{\partial P}{\partial T})_V}{(\frac{\partial P}{\partial V})_T} \frac{(\frac{\partial S}{\partial V})_T}{(\frac{\partial S}{\partial T})_V} \right] \\
&= \left(\frac{\partial P}{\partial V} \right)_T \left[1 + \left(\frac{\partial V}{\partial T} \right)_P \frac{T}{C_V} \left(\frac{\partial S}{\partial V} \right)_T \right]. \tag{70}
\end{aligned}$$

Therefore, the ratio $(\partial P/\partial V)_S/(\partial P/\partial V)_T$ in Eq. (69) is given as

$$\frac{(\frac{\partial P}{\partial V})_S}{(\frac{\partial P}{\partial V})_T} = 1 + T \left(\frac{\partial V}{\partial T} \right)_P \frac{1}{C_V} \left(\frac{\partial S}{\partial V} \right)_T. \tag{71}$$

The specific heat $C_V(T)$ is calculated with the use of Eq. (A.1), and exhibits the following T dependence at $T_Q < T \ll E_0$, with T_Q being the transition temperature of the quadrupole ordering:

$$C_V(T) \simeq C_0 \left(1 - a_5 \sqrt{T/E_0} \right), \tag{72}$$

as shown in Fig. 13(a). Therefore, by integrating the relation $(\partial S/\partial T)_V = C_V(T)/T$ with respect to T , the T dependence of the entropy $S(T)$ is given by

$$S(T) \simeq S(T_Q) + C_0 \left[\ln \frac{T}{T_Q} - 2a_5 \left(\sqrt{\frac{T}{E_0}} - \sqrt{\frac{T_Q}{E_0}} \right) \right]. \tag{73}$$

Then, the second term of Eq. (71) is of the order of $O(T/E_0)$ within a logarithmic accuracy in T , because the fundamental energy scale determining the low energy physics is given by E_0 . Therefore, considering that the T dependence of physical quantities is scaled by E_0 at $T \ll E_0$, the second term of Eq. (71) is neglected compared to the first term at $T \ll E_0$, giving $(\partial P/\partial V)_S/(\partial P/\partial V)_T \simeq 1$. Namely, $C_P(T)$ can be approximated by $C_V(T)$ so long as the T dependence of the leading order, i.e., $O(\sqrt{T/E_0})$, is concerned.

Figure 13 shows the T dependence of the specific heat $C_V(T)$ for the two channel [(a)] and single channel [(b)] in the unit of k_B , the Boltzmann constant. In the case of two-channel ($M = 2$), the specific heat $C_V(T)$ at $T_Q < T \ll E_0$ can be well fitted by

$$C_V = C_0 \left(1 - a_5 \sqrt{T/E_0} \right), \tag{74}$$

as can be seen in Fig. 13(a). This T dependence in $C(T)$ was observed both in $\text{PrV}_2\text{Al}_{20}$ ¹⁾ and $\text{PrIr}_2\text{Zn}_{20}$.²⁾ T_Q in Fig. 13(a) is the transition temperature for the antiferro quadrupole ordering, and is estimated by the RPA for the response function

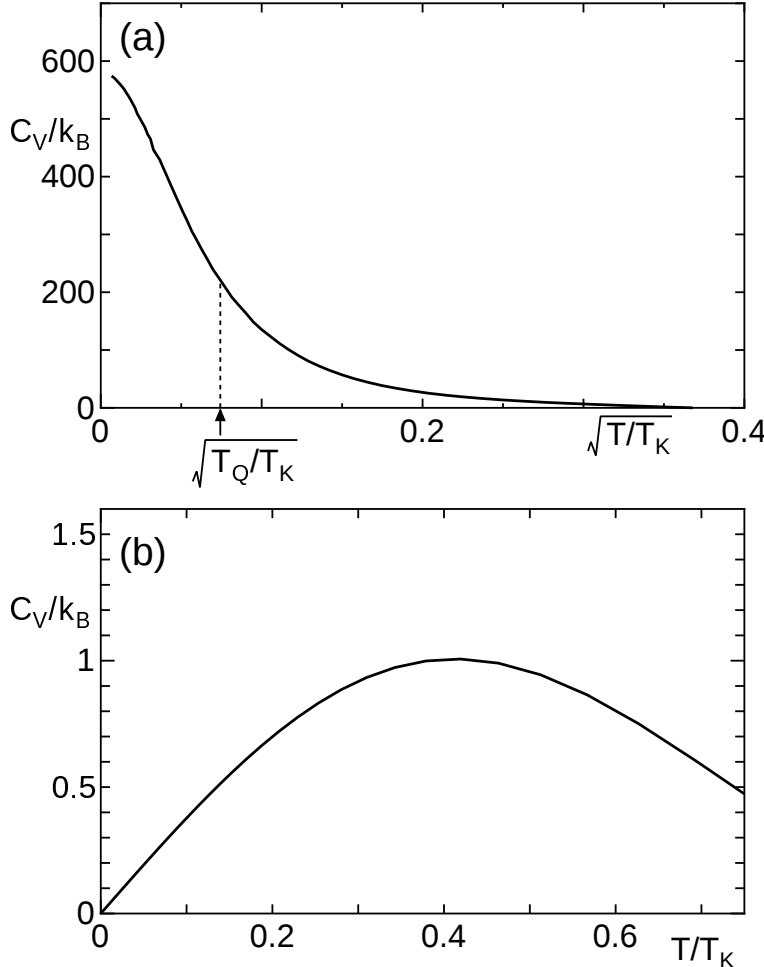


Fig. 13. T dependence of the specific heat C_V for (a) two-channel case and (b) single-channel case. T_Q in (a) is the transition temperature for the antiferro quadrupole ordering. Note that the regions of T/T_K presented in (a) and (b) are quite different, so that $T/T_K = 0.1$ corresponds to $\sqrt{T/T_K} \simeq 0.3$.

of pseudo-boson density which represents the quadrupole density arising from Γ_3 non-Kramers doublet. (Details of calculation will be discussed elsewhere.) However, this result apparently breaks the third law of thermodynamics if it would be applied down to $T = 0$. This deficiency may be avoided by taking into account the existence of ordered states such as quadrupole order, superconducting order, magnetic order and so on, while the quadrupole order is the most promising in the present model. On the other hand, in the case of single channel ($M = 1$), the specific heat $C_V(T)$ is proportional to T as shown in Fig. 13(b), manifesting the Fermi liquid state.

7. Magnetic Susceptibility of Conduction Electrons

In this section, we calculate the magnetic susceptibility χ_m which corresponds to the channel susceptibility in the present model given by Eqs. (2)-(5) or (6) and (7). The conduction-electrons component of the magnetic susceptibility described by the diagram shown in Fig. 14 is larger than that from the slave fermion. To the leading order in $1/N$, the χ_m is given explicitly by

$$\chi_m(\mathbf{q}) = \chi_m^{(1)}(\mathbf{q}) + \chi_m^{(2)}(\mathbf{q}) \quad (75)$$

$$\chi_m^{(1)}(\mathbf{q}) = -\mu_{\text{eff}}^2 T \sum_{\epsilon_n} \frac{1}{N_L} \sum_{\mathbf{k}, \tau} G_{\mathbf{k}\tau\sigma}^{(1)}(i\epsilon_n) G_{\mathbf{k}+\mathbf{q}\tau\sigma}^{(1)}(i\epsilon_n) \quad (76)$$

$$\begin{aligned} \chi_m^{(2)}(\mathbf{q}) = & -\mu_{\text{eff}}^2 T^2 \sum_{\epsilon_{n_1}, \epsilon_{n_2}} \frac{1}{N_L^2} \sum_{\mathbf{k}_1, \mathbf{k}_2, \tau} G_{\mathbf{k}_1\tau\sigma}^{(1)}(i\epsilon_{n_1}) G_{\mathbf{k}_2\tau\sigma}^{(1)}(i\epsilon_{n_2}) \Gamma_{\mathbf{q}}^{(0)}(i\epsilon_{n_1}, i\epsilon_{n_2}; 0) \\ & \times G_{\mathbf{k}_2\tau\sigma}^{(1)}(i\epsilon_{n_2}) G_{\mathbf{k}+\mathbf{q}\tau\sigma}^{(1)}(i\epsilon_{n_2}), \end{aligned} \quad (77)$$

where μ_{eff} is the effective magnetic moment of the conduction electrons with Γ_8 symmetry.

Figure 15 shows the T dependence of $\chi_m = \chi_m(\mathbf{q} = 0)$. In the case of single channel, χ_m is given in the form

$$\chi_m = \chi_m(T = 0) [1 - a_6 (T/E_0)^2]. \quad (78)$$

In the case of two-channel, χ_m is given in the form

$$\chi_m = \chi_m(T = 0) \left(1 - a_7 \sqrt{T/E_0} \right). \quad (79)$$

In the non-Fermi liquid system, the magnetic susceptibility is suppressed by the non-Fermi liquid imaginary part of the self-energy (ISE). But both of the Fermi liquid ISE and the non-Fermi liquid ISE is zero at zero temperature. Therefore, χ_m in the non-Fermi liquid system is rapidly increase compared with that of the Fermi liquid system. The theoretical result, Eq. (79), qualitatively explain the T dependence of the $\text{PrV}_2\text{Al}_{20}$ ¹⁾ and $\text{PrIr}_2\text{Zn}_{20}$.²⁾ However, the cusp in the case of two channel at low temperature is far smaller than that observed in experiments.

This quantitative discrepancy with experiments may be cured by taking into account the following two aspects which are not included in the model Hamiltonian Eq. (6). First of all, in our calculation, we have neglected the excited states in CEF of $4f^2$ -configuration including a magnetic degrees of freedom. In other words, we have calculated the magnetic susceptibility of quasiparticles near the Fermi level. However,

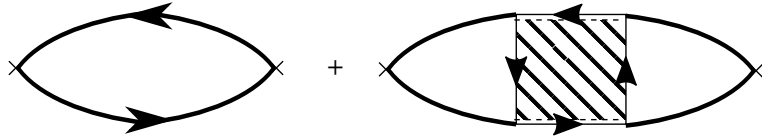


Fig. 14. Feynman diagrams giving the magnetic susceptibility. The first and the second terms represent for $\chi_m^{(1)}$ and $\chi_m^{(2)}$, respectively.

there also arises the magnetic susceptibility through the virtual hopping processes including the excited CEF states i.e., the Van Vleck term which gives a considerable contribution. Indeed, it has been shown by the numerical renormalization group (NRG) calculations²⁵⁾ that the magnetic susceptibility of the impurity model for UPt₃ with singlet CEF ground state in f^2 -configuration consists of the Van Vleck type contribution and that of quasiparticles, the latter of which is not enhanced while the specific heat coefficient is highly enhanced. It has also been shown by the slave-boson mean-field calculation²⁶⁾ that the quasiparticles' contribution to magnetic susceptibility is not enhanced if the CEF ground state is singlet in f^2 -configuration even though the effective mass of quasiparticles is highly enhanced.

Secondly, it has been shown by the NRG calculation for the two-channel impurity Kondo model²⁷⁾ that the perturbation breaking a particle-hole symmetry, such as the repulsive interaction among conduction electrons, gives rise to the same divergent behavior in the channel susceptibility (the spin-orbital susceptibility in the present model) as the spin susceptibility (the quadrupolar susceptibility in the present model). This aspect is expected to be succeeded to the case of two-channel lattice system.

8. Concluding Remarks

We have shown that the non-Fermi-liquid properties observed in PrV₂Al₂₀ and PrIr₂Zn₂₀ can be understood on the basis of the two-channel Anderson lattice model with the use of the $1/N$ -expansion formalism à la Nagoya which had been confirmed to be valid for properly taking strong correlation effects into account. This Anderson lattice model simulates the heavy fermion systems with Γ_3 non-Kramers doublet CEF ground state in f^2 -configuration, such as PrA₂Al₂₀ ($A = \text{Ti}, \text{V}$) and PrIr₂Zn₂₀. Results obtained in the present study are summarized as follows:

- 1) The imaginary part of the conduction electrons, which has already been derived in Ref. 10 as given by Eq. (1) to the order of $O(1/N)$, explains the non-Fermi-liquid T

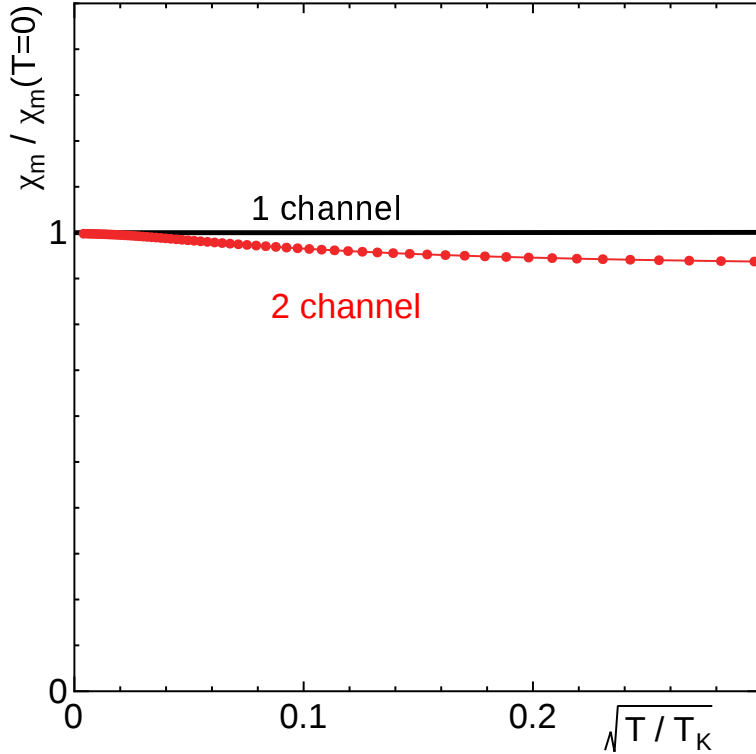


Fig. 15. T dependence of the magnetic susceptibility for two-channel case (red line with dots) and single-channel case (black line without dots).

dependence of the resistivity $\rho(T)$ observed in $\text{PrV}_2\text{Al}_{20}$ and $\text{PrIr}_2\text{Zn}_{20}$. In particular, it turned out for the first time that $\rho(T)$ has a scaling form $\rho(T) = R(T/T_0)$ where T_0 , the crossover temperature at which T dependence of $\rho(T)$ changes from $\propto \sqrt{T}$ to $\propto T^\eta$ (with $\eta < 1/2$), depends on pressure through the change of the hybridization between f - and conduction electrons.

2) It has been shown explicitly that the DMFT cannot predict correct behavior of $\rho(T)$ when applied to the multichannel Anderson lattice model or multichannel Kondo lattice model because it is only valid in the limit of infinite spatial dimension, $d \rightarrow \infty$, in which T_k^* in Eq. (1) vanishes in proportion to $1/d$, giving an unphysical result $\lim_{T \rightarrow 0} \rho(T) \neq 0$. On the other hand, it works correctly when applied to the case of the single-channel Anderson lattice model with $M = 1$ for which the second term in Eq. (1) vanishes, accidentally killing the unphysical effect.

3) The T dependence of the chemical potential $\mu(T)$ exhibits \sqrt{T} dependence as given by Eq. (55) in rather wide temperature region $T_x < T < 0.02T_K$, with the lower

$t \equiv T/E_0$ ($T_x/E_0 \ll t \ll 1$)	Single Channel	Two Channel
Electrical Resistivity	$a_1 t^2$	$a_2/(1 + b/t)$
Chemical Potential	$\mu_0(1 + a_3 t^2)$	$\mu_0(1 + a_4 \sqrt{t})$
Specific Heat	γT	$c_0(1 - a_5 \sqrt{t})$
Magnetic Susceptibility	$\chi_0(1 - a_6 t^2)$	$\chi_0(1 - a_7 \sqrt{t})$

Table I. T dependence of physical quantities in the case of single channel and two channel, in the region $T_x/E_0 \ll t \ll 1$ with $t \equiv T/E_0$.

crossover temperature $T_x/T_K \simeq 0.0008$ at which T dependence of $\rho(T)$ changes from $\propto T$ to $\propto \sqrt{T}$ as T increases for the typical parameter set adopted, i.e., $V/D = 0.3$. The specific heat $C(T)$ and the magnetic susceptibility $\chi_m(T)$ exhibit similar T dependence given by Eqs. (74) and (79), respectively, or as shown in Table I. The T dependence of $C(T)$ is nicely fitted to experimental results observed in $\text{PrV}_2\text{Al}_{20}$ and $\text{PrIr}_2\text{Zn}_{20}$ above the transition temperatures of the antiferro- or ferro-quadrupole order and the superconductivity.^{2,17)}

On the other hand, there remain some problems to be resolved. Namely, $\lim_{T \rightarrow 0} C(T) \neq 0$ which apparently breaks the Nernst law, and the anomaly of $\chi_m(T)$ is too small compared to that observed in experiments of $\text{PrV}_2\text{Al}_{20}$. For the former problem, we have to take into account the existence of ordered states which can release the entropy below their transition temperatures. For the latter problem, as discussed in Sect. 7, we have to extend the model Hamiltonian to take into account the effects that are beyond the present model, or consider the higher order terms in $1/N$ -expansion as performed in the impurity version of the multichannel Anderson model discussed in Ref. 28. It is also left for future study to investigate various ordered states in the two-channel Anderson lattice model.

Acknowledgments

We are grateful to A. Sakai, S. Nakatsuji, and K. Matsubayashi, and T. Onimaru, K. Izawa, and Y. Machida for stimulating discussions on the experimental results of $\text{Pr}A_2\text{Al}_{20}$ ($A = \text{V}, \text{Ti}$) and $\text{PrIr}_2\text{Zn}_{20}$, respectively. In particular, we acknowledge T. Onimaru for allowing us to use the experimental data of the resistivity in $\text{PrIr}_2\text{Zn}_{20}$ prior to publication. This work is supported by a Grant-in-Aid for Scientific Research on Innovative Areas “Topological Quantum Phenomena” (No. 22103003) from the Min-

istry of Education, Culture, Sports, Science and Technology and by a Grant-in-Aid for Scientific Research (No. 25400369) from the Japan Society for the Promotion of Science.

Appendix A: Formalism for Calculating the Specific Heat

In this appendix, we show how the specific heat C_V is calculated.

The specific heat C_V per site is given by

$$C_V = \frac{1}{N_L} \left(\frac{\partial \langle H \rangle}{\partial T} \right)_{V,N}, \quad (\text{A}\cdot1)$$

where $\langle H \rangle$ is the internal energy which is the average of the Eq. (6), with $\varepsilon_{\mathbf{k}\tau\bar{\tau}} = 0$,

$$\langle H \rangle = E_c + E_f + E_v, \quad (\text{A}\cdot2)$$

where

$$E_c = \sum_{\mathbf{k}, \tau, \sigma} \varepsilon_{\mathbf{k}} \langle c_{\mathbf{k}\tau\sigma}^+ c_{\mathbf{k}\tau\sigma} \rangle, \quad (\text{A}\cdot3)$$

$$E_f = \sum_{i, \tau} \varepsilon_{\Gamma_3}^{(0)} \langle b_{i\tau}^+ b_{i\tau} \rangle + \sum_{i, \sigma} \varepsilon_{\Gamma_7}^{(0)} \langle f_{i\sigma}^+ f_{i\sigma} \rangle, \quad (\text{A}\cdot4)$$

and

$$E_v = \frac{1}{\sqrt{N_L}} \sum_{i, \mathbf{k}, \tau, \sigma} (V \langle c_{\mathbf{k}\tau\bar{\sigma}}^+ f_{i\sigma}^+ b_{i\tau} \rangle e^{-i\mathbf{k}\mathbf{R}_i} + \text{h.c.}) . \quad (\text{A}\cdot5)$$

With the use of $1/N$ -expansion, E_c and E_f are given by

$$E_c = \sum_{\mathbf{k}, \tau, \sigma} \varepsilon_{\mathbf{k}} \int d\epsilon f(\epsilon) \frac{-1}{\pi} \text{Im} G_{\mathbf{k}\tau\sigma}^{(1)}(\epsilon + i0_+), \quad (\text{A}\cdot6)$$

and

$$E_f = \sum_i \varepsilon_{\Gamma_3}^{(0)} n_{\text{slave boson}} + \sum_i \varepsilon_{\Gamma_7}^{(0)} n_{\text{pseudo fermion}}, \quad (\text{A}\cdot7)$$

where the Green function $G_{\mathbf{k}\tau\sigma}^{(1)}(\epsilon + i0_+)$ is given by Eq. (49), $n_{\text{slave fermion}}$ and $n_{\text{pseudo boson}}$ are given below Eq. (46). The explicit Feynman diagrams for E_v are shown in Fig. A1, and its analytic form is given as follows:

$$\begin{aligned} E_v &= 2 \frac{1}{\sqrt{N_L}} \sum_{\sigma} \sum_{\tau} \sum_{i, \mathbf{k}} V \langle c_{\mathbf{k}\tau\bar{\sigma}}^+ f_{i\sigma}^+ b_{i\tau} \rangle e^{-i\mathbf{k}\mathbf{R}_i} \\ &= -2 \frac{1}{\sqrt{N_L}} \sum_{\sigma} \sum_{\tau} \sum_{i, \mathbf{k}} V \langle T_{\tau} f_{i\sigma}^+(-0_+) b_{i\tau}(-0_+) c_{\mathbf{k}\tau\bar{\sigma}}^+(0) \rangle e^{-i\mathbf{k}\mathbf{R}_i} \\ &= -2 \sum_{\sigma} \sum_{\tau} \sum_{\mathbf{k}} T \sum_{\epsilon_n} e^{-i\epsilon_n 0_+} G_{\mathbf{k}\tau\sigma}^{(1)}(i\epsilon_n) \Sigma_{\mathbf{k}\tau\sigma}(i\epsilon_n) \end{aligned}$$

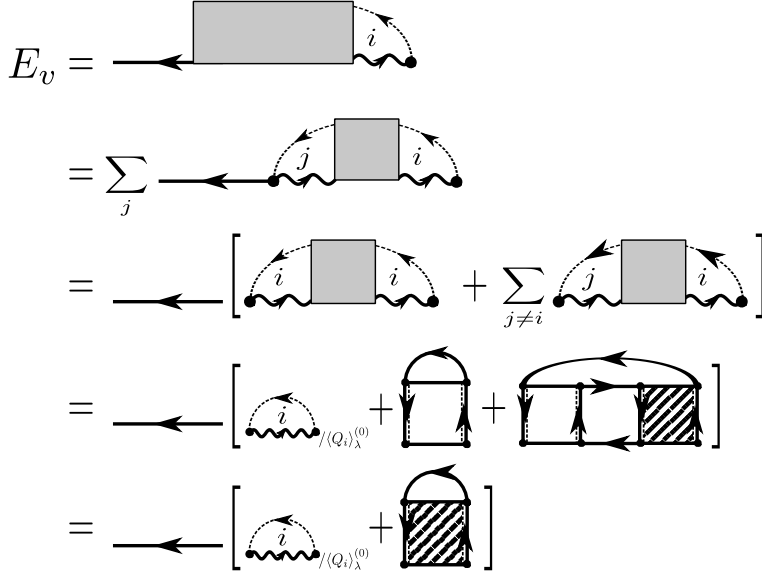


Fig. A.1. Feynman diagram representation for E_v . Closed circle represents the hybridization V . Solid line with arrow represents the Green function of conduction electrons, $G_{\mathbf{k}\tau\sigma}^{(1)}(i\epsilon_n)$, the dotted line with arrow represents the Green function of pseudo bosons, $B_{i\tau}^{(0)}(i\nu_m)$, the wavy line with arrow represents the Green function of the slave fermions, $F_{i\sigma}^{(1)}(-i\epsilon_n + i\nu_m)$, and shaded square represents the vertex $\Gamma_q^{(0)}$ given by Fig. 3(b).

$$= -2 \sum_{\sigma} \sum_{\tau} \sum_{\mathbf{k}} \int d\epsilon f(\epsilon) \frac{-1}{\pi} \text{Im} \left[G_{\mathbf{k}\tau\sigma}^{(1)}(\epsilon + i0_+) \Sigma_{\mathbf{k}\tau\sigma}(\epsilon + i0_+) \right]. \quad (\text{A.8})$$

Appendix B: Numerical Recipe

In this appendix, we show a recipe for numerical calculations for the integration with respect to real frequency ϵ , as in Eq. (47). Explicitly, we use the trapezoidal rule:

$$\int_{-\infty}^{\infty} d\epsilon A(\epsilon) \simeq \sum_{i=-M}^M \Delta\epsilon_i A(\epsilon_i). \quad (\text{B.1})$$

To take finer meshes of summation in the low frequency region, we adopt a weighted mesh for summation over ϵ_i with the use of ϵ_i and $\Delta\epsilon_i$ given by

$$\epsilon_i = \text{sgn}(i) \epsilon_1 \frac{r^{|i|} - 1}{r - 1}, \quad (\text{B.2})$$

and

$$\Delta\epsilon_i = \begin{cases} \epsilon_1 & (i = 0) \\ \frac{\epsilon_1}{2} r^{|i|-1} (r + 1) & (i \neq 0), \end{cases} \quad (\text{B.3})$$

where $\text{sgn}(x)$ is the sign function given by

$$\text{sgn}(x) \equiv \begin{cases} 1 & (x > 0) \\ 0 & (x = 0) \\ -1 & (x < 0). \end{cases} \quad (\text{B.4})$$

Note that the term with $\epsilon_0 = 0$ and $\Delta\epsilon_0 = \epsilon_1$ is taken into account. For explicit calculations, we adopt parameters as $M = 100$, $\epsilon_1 = 10^{-3}D$, $\epsilon_M = 2D$ and $r = 1.04647534$, where r is determined by the relation

$$\epsilon_M = \epsilon_1 \frac{r^M - 1}{r - 1}. \quad (\text{B.5})$$

References

- 1) A. Sakai and S. Nakatsuji, J. Phys. Soc. Jpn. **80**, 063701 (2011);
S. Nakatsuji, private communications.
- 2) T. Onimaru, K. T. Matsumoto, Y. F. Inoue, K. Umeo, T. Sakakibara, Y. Karaki, M. Kubota, and T. Takabatake, Phys. Rev. Lett. **106**, 177001 (2011);
T. Onimaru, K. T. Matsumoto, Y. F. Inoue, K. Umeo, Y. Saiga, Y. Matsushita, R. Tamura, K. Nishimoto, I. Ishii, T. Suzuki, and T. Takabatake, J. Phys. Soc. Jpn. **79**, 033704 (2010);
T. Onimaru, private communications.
- 3) Y. Sato, H. Morodomi, K. Ienaga, Y. Inagaki, T. Kawae, H. S. Suzuki, and T. Onimaru, J. Phys. Soc. Jpn. **79**, 093708 (2010).
- 4) P. Nozières and A. Blandin, J. Physique **41**, 193 (1980).
- 5) D. L. Cox, Phys. Rev. Lett. **59**, 1240 (1987).
- 6) See for example, D. L. Cox and A. Zawadowski, Exotic Kondo Effects in Metals: Magnetic Ions in a Crystalline Electric Field and Tunneling Centres (Taylor & Francis, London, 2002), Sect. 5.
- 7) Y. Ōno, T. Matsuura and Y. Kuroda, Physica C **159**, 878 (1989).
- 8) Y. Ōno, T. Matsuura and Y. Kuroda, J. Phys. Soc. Jpn. **60**, 3475 (1991).
- 9) Y. Ōno, J. Phys. Soc. Jpn. **67**, 2197 (1998).
- 10) A. Tsuruta, A. Kobayashi, K. Deguchi, Y. Ōno, T. Matsuura and Y. Kuroda, J. Phys. Soc. Jpn. **68**, 1067 (1999).
- 11) A. Tsuruta, A. Kobayashi, T. Matsuura and Y. Kuroda, J. Phys. Soc. Jpn. **69**, 3342 (2000).
- 12) Y. Nishida, A. Tsuruta, and K. Miyake, J. Phys. Soc. Jpn. **75**, 064706 (2006).
- 13) D. Jaccard, H. Wilhelm, K. Alami-Yadri, and E. Vargo, Physica B **259-261**, 1 (1999).
- 14) A. T. Holmes, D. Jaccard, and K. Miyake, Phys. Rev. B **69**, 024508 (2004).
- 15) B. Barbara, J. Beille, B. Cheaito, J. M. Laurant, M. F. Rossignol, A. Waintal, and S. Zemirli, J. Phys. (Paris) **48**, 635 (1987).
- 16) M. Jarrell, H. Pang, D.L. Cox, F. Anders and A. Chatopadhyay, Physica B**230-232**, 557 (1997).

- 17) K. Matsubayashi, T. Tanaka, A. Sakai, S. Nakatsuji, Y. Kubo, and Y. Uwatoko, Phys. Rev. Lett. **109**, 187004 (2012).
- 18) P. Coleman, Phys. Rev. B **29**, 3035 (1984).
- 19) B. Jin and Y. Kuroda, J. Phys. Soc. Jpn. **57**, 1687 (1988).
- 20) T. Onimaru: private communication.
- 21) S. Nakatsuji: private communication.
- 22) K. Izawa: private communication.
- 23) S. Hoshino, J. Otsuki, and Y. Kuramoto, J. Phys. Soc. Jpn. **82**, 044707 (2013).
- 24) H. Maebashi and H. Fukuyama, J. Phys. Soc. Jpn. **66**, 3577 (1997).
H. Maebashi and H. Fukuyama, J. Phys. Soc. Jpn. **67**, 242 (1998).
- 25) S. Yotsuhashi, K. Miyake, and H. Kusunose, Physica B **312-313**, 100 (2002).
- 26) H. Ikeda and K. Miyake, J. Phys. Soc. Jpn. **66**, 3714 (1997).
- 27) H. Kusunose, K. Miyake, Y. Shimizu, and O. Sakai, Phys. Rev. Lett. **76**, 271 (1996).
- 28) A. Tsuruta, Y. Ōno, T. Matsuura and Y. Kuroda, J. Phys. Soc. Jpn. **67**, 2346 (1998).